The effects of multi-echo fMRI combination and rapid T_2*-mapping on offline and real-time BOLD sensitivity

NeuroImage 238 (2021) 118244

Contents lists available at ScienceDirect

NeuroImage

journal homepage: www.elsevier.com/locate/neuroimage

The effects of multi-echo fMRI combination and rapid T_2*-mapping on offline and real-time BOLD sensitivity

Stephan Heunis[a,b,c,d,*], Marcel Breeuwer[e,f], César Caballero-Gaudes[g], Lydia Hellrung[h], Willem Huijbers[a,i], Jacobus FA Jansen[a,j,k], Rolf Lamerichs[a,b,i], Svitlana Zinger[a,b], Albert P Aldenkamp[a,b,k,l,m]

[a] Department of Electrical Engineering, Eindhoven University of Technology, Eindhoven, the Netherlands
[b] Department of Research and Development, Epilepsy Centre Kempenhaeghe, Heeze, the Netherlands
[c] Institute of Neuroscience and Medicine, Brain & Behaviour (INM-7), Research Center Jülich, Germany
[d] Department of Psychology, Education and Child studies, Erasmus School of Social and Behavioral Sciences, Erasmus University Rotterdam, the Netherlands
[e] Department of Biomedical Engineering, Eindhoven University of Technology, Eindhoven, the Netherlands
[f] Philips Healthcare, Best, the Netherlands
[g] Basque Center on Cognition, Brain and Language, San Sebastian, Spain
[h] Zurich Center for Neuroeconomics, Department of Economics, University of Zurich, Switzerland
[i] Philips Research, Eindhoven, the Netherlands
[j] Department of Radiology and Nuclear Medicine, Maastricht University Medical Centre, Maastricht, the Netherlands
[k] School for Mental Health and Neuroscience, Maastricht, the Netherlands
[l] Laboratory for Clinical and Experimental Neurophysiology, Neurobiology and Neuropsychology, Ghent University Hospital, Ghent, Belgium
[m] Department of Neurology, Maastricht University Medical Center, Maastricht, the Netherlands

ARTICLE INFO

Keywords:
Real-time
Multi-echo
Functional magnetic resonance imaging
Neurofeedback
Adaptive paradigms
Methods development
Finger tapping
Motor
Emotion processing
Amygdala
Task
Resting state

ABSTRACT

A variety of strategies are used to combine multi-echo functional magnetic resonance imaging (fMRI) data, yet recent literature lacks a systematic comparison of the available options. Here we compare six different approaches derived from multi-echo data and evaluate their influences on BOLD sensitivity for offline and in particular real-time use cases: a single-echo time series (based on Echo 2), the real-time T_2*-mapped time series (T_2*FIT) and four combined time series (T_2*-weighted, tSNR-weighted, TE-weighted, and a new combination scheme termed T_2*FIT-weighted). We compare the influences of these six multi-echo derived time series on BOLD sensitivity using a healthy participant dataset ($N = 28$) with four task-based fMRI runs and two resting state runs. We show that the T_2*FIT-weighted combination yields the largest increase in temporal signal-to-noise ratio across task and resting state runs. We demonstrate additionally for all tasks that the T_2*FIT time series consistently yields the largest offline effect size measures and real-time region-of-interest based functional contrasts and temporal contrast-to-noise ratios. These improvements show the promising utility of multi-echo fMRI for studies employing real-time paradigms, while further work is advised to mitigate the decreased tSNR of the T_2*FIT time series. We recommend the use and continued exploration of T_2*FIT for offline task-based and real-time region-based fMRI analysis. Supporting information includes: a data repository (https://dataverse.nl/dataverse/rt-me-fmri), an interactive web-based application to explore the data (https://rt-me-fmri.herokuapp.com/), and further materials and code for reproducibility (https://github.com/jsheunis/rt-me-fMRI).

1. Introduction

In functional magnetic resonance imaging (fMRI), T_2*-weighted MRI sequences use the blood oxygen level-dependant (BOLD) signal as a proxy for neuronal activity. Our ability to infer accurate information about neuronal processes is influenced by the sensitivity with which we can capture these BOLD changes and subsequently delineate its sources of variance. Improved sensitivity is particularly important for real-time use cases, such as adaptive experimental paradigms, real-time quality control, or fMRI neurofeedback, where BOLD changes are quantified and used as they are acquired without the benefit of a full dataset or the requisite amount of post-processing time. It is well known that optimum sensitivity of single-echo fMRI is achieved at an echo time (TE) close to the apparent tissue T_2*-value at baseline (Menon et al., 1993), which also underlies an inherent drawback of T_2*-weighted sequences. Location-specific BOLD sensitivity is suboptimal since T_2* varies across tissue types and brain regions (Peters et al., 2007), which can result in spatial variability in the detection of task-related activation patterns.

* Corresponding author.
E-mail address: s.heunis@fz-juelich.de (S. Heunis).

https://doi.org/10.1016/j.neuroimage.2021.118244.
Received 8 December 2020; Received in revised form 11 April 2021; Accepted 4 June 2021
Available online 8 June 2021.

Furthermore, magnetic susceptibility gradients on a macroscopic level result in image defects such as signal dropout and distortion, which is pronounced in the ventromedial prefrontal, orbitofrontal, the medial temporal and the inferior temporal lobes (Devlin et al., 2000). Additionally, the complex interplay of blood flow, blood volume and magnetic susceptibility effects can be influenced strongly by system- and participant-level noise sources, thus confounding the BOLD signal.

An advancement that has shown promise in making inroads into these drawbacks is multi-echo fMRI. Several studies have shown benefits of offline denoising based on multi-echo independent component analysis (MEICA; Kundu et al., 2012) for both resting state (e.g. Olafsson et al., 2015; Dipasquale et al., 2017) and task-based fMRI data (e.g., Lombardo et al., 2016; Gonzalez-Castillo et al., 2016; Moia et al., 2020). Echo combination via weighted summation is a critical step in multi-echo post-processing that has been reported to increase temporal signal-to-noise ratio, decrease signal drop-out, and improve activation extent for task-analysis (Poser et al., 2006). Posse et al. (1999) proposed several echo combination schemes, including simple echo summation (i.e. equal weights) and weighting echoes by their relative expected BOLD contrast contribution (i.e. T_2^*), which would require a numerical or fitted estimation of T_2^*. Other possible weighting schemes include optimised scalar weights, TE-weighted combination, and tSNR-weighted combination (also termed the PAID method) proposed by Poser et al. (2006). A theoretical framework for optimizing multi-echo combination has also been proposed by Gowland and Bowtell (2007). However, the relative benefits of all available combination schemes remain unclear.

With access to multiple data samples along the decay curve, multi-echo allows quantification of the effective transverse relaxation parameter T_2^* (decay time) or R_2^* (its inverse, decay rate), and S_0 (initial net magnetization). This form of quantitative T_2^*-mapping (such as described by Weiskopf et al., 2013) acquires multiple closely spaced echoes followed by a data fitting procedure that yields a static, baseline T_2^*-map. In the context of functional imaging, however, temporal or per-volume T_2^*-mapping is also feasible, with the core benefit being the separation and quantification of T_2^* and S_0 changes (from baseline) during stimulated neuronal activation. Such real-time use cases of multi-echo data have been reported, starting with Posse et al.'s (1998) single-shot, multi-echo spectroscopic imaging sequence that quantified region-specific T_2^* changes during olfactory and visual tasks, and which reported a larger functional contrast (up to 20% increase in the visual cortex) compared to standard EPI data. Several developments followed, including measuring single-event related brain activity (Posse et al., 2001), whole brain T_2^*-mapping at 1.5T using a linear combination of echoes (Hagberg et al., 2002), later with added gradient compensation (Posse et al., 2003), and a multi-echo EPI sequence at 3T with real-time distortion correction (Weiskopf et al., 2005). Rapid T_2^*-mapping has also been a useful tool in studying the interplay between cerebral blood flow, blood volume and blood oxygenation, particularly in combination with contrast agents (see, for example: Scheffler et al., 1999; Schulte et al., 2001; Pears et al., 2003). In real-time fMRI neurofeedback, some examples of multi-echo use are reported specifically for improving signal gains in regions such as the amygdala, including Posse et al. (2003) which uses T_2^*-weighted echo summation and Marxen et al. (2016), which uses scalar TE-dependant weights preselected to yield an average T_2^*-value of 30 ms in the amygdala.

Although methodological studies have reported the benefits of multi-echo fMRI combination, a comprehensive evaluation of its practical benefits is lacking. Specifically, a variety of combination methods exist that can lead to both offline and real-time improvements in BOLD sensitivity, but there has been no systematic comparison between such methods. Additionally, per-volume T_2^*-mapping forms a necessary step in established multi-echo-based methods, but recent literature has not explored its value for task fMRI analysis. Consequently, this study has two main goals: (1) to explore the differences in BOLD sensitivity, both offline and per-volume, between time series of standard single echo EPI, per-volume estimated T_2^*FIT, and multi-echo-combined time series (including tSNR-weighted, T_2^*, TE-weighted, and T_2^*FIT-weighted); and (2) to explore the T_2^*FIT time series as an alternative to single-echo or multi-echo-combined time series for offline and real-time fMRI analysis. We investigate these aims for whole brain data in separate task paradigms, eliciting responses to motor and emotion processing tasks and mental versions thereof, and during resting state. To quantify differences, we employ several metrics such as tSNR, task activity effect size, region-of-interest based temporal percentage signal change (tPSC), functional contrast, and temporal contrast-to-noise ratio (tCNR).

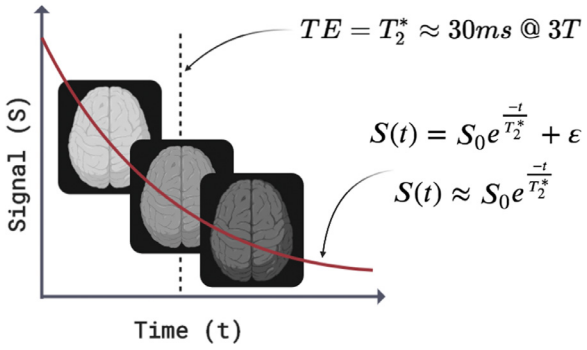

Fig. 1. A representation of mono-exponential signal decay showing diminishing image intensity along three echoes. The second echo is sampled at the optimum echo time equal to average grey matter T_2^*, standard for single echo fMRI. The equation for the red, mono-exponential decay curve is provided (Eq. (1)).

2. Multi-echo fMRI relaxation and combination

Multi-echo fMRI sequences acquire a slice or multiple slices of a functional image at discrete echo times (TE) after a single transverse excitation pulse of the scanner. All slices of a whole brain image are acquired within the standard repetition time (TR) which then yields multiple echoes per volume. The relaxation of the fMRI signal in a given voxel after transverse excitation, assuming a mono-exponential decay model, is given as:

$$S(t) = S_0 \cdot e^{\frac{-t}{T_2^*}} + \varepsilon = S_0 \cdot e^{-t \cdot R_2^*} + \varepsilon \tag{1}$$

with $S(t)$ being the time-decaying fMRI signal, S_0 being the tissue magnetization directly after transverse excitation, and T_2^* being the local tissue transverse relaxation (i.e. decay time) constant (the inverse of the decay rate, R_2^*). Per-voxel estimates of S_0 and T_2^* (depicted below in Fig. 1) can be derived using a log-linear regression estimation and the available echo times (t_1 to t_n, where *pinv* is the pseudo-inverse log the natural logarithm):

$$\begin{bmatrix} \log(S_0) \\ R_2^* \end{bmatrix} = pinv\left(\begin{bmatrix} 1 - t_1 \\ 1 - t_2 \\ \vdots \\ 1 - t_n \end{bmatrix}\right) * \begin{bmatrix} \log\left(S(t_1)\right) \\ \log\left(S(t_2)\right) \\ \vdots \\ \log\left(S(t_n)\right) \end{bmatrix} \tag{2}$$

The mathematics of all widely used multi-echo combination schemes are based on the underlying concepts of data weighting, summation and averaging. In the supplementary online material, we provide a thorough background of these concepts along with explanatory equations S1 through S6. Importantly, the multi-echo combination schemes presented below use the convention of weighted summation with normalized weights. This implies that (1) all weights are normalized such that their sum equals 1, then (2) each normalized weight is multiplied by its corresponding data point, then (3) these products are summed to produce the weighted summation.

Simple echo summation

Simple echo summation assumes equal weights for all echoes (totalling N), which is calculated for an individual echo n as:

$$w_n^{SUM} = \frac{1}{N} \tag{3}$$

tSNR-weighted combination

The PAID method put forward by Poser et al. (2006) uses the voxel-based tSNR measured at each echo ($tSNR_n$) as the weights:

$$w_n^{tSNR} = \frac{tSNR_n \cdot TE_n}{\sum_{i=1}^{N} tSNR_i \cdot TE_i} \tag{4}$$

TE-weighted combination

Purely using each echo's echo time, TE_n, as the weight for that echo has also been suggested (Posse et al., 1999). In this case, the same scalar value is used as the weighting factor for all voxels of a specific echo: iom

$$w_n^{TE} = \frac{TE_n}{\sum_{i=1}^{N} TE_i} \tag{5}$$

Similarly, a range of scalar values can be used as echo-dependant weighting factors, usually optimised according to study-specific criteria. For example, Marxen et al. (2016) selected scalar weights in order to yield an average T_2^* value of 30 ms in their region of interest (the amygdala). In such a case, the predefined scalar weights $\{SW_1, SW_2, \ldots, SW_N\}$ can be normalized as:

$$w_n^{SW} = \frac{SW_n}{\sum_{i=1}^{N} SW_i} \tag{6}$$

T_2^*-weighted combination

The T_2^*-weighted combination scheme used by Posse et al. (1999) and termed "optimal combination" by Kundu et al. (2012), calculates the individual echo weights w_n per voxel as:

$$w_n^{T_2^*} = \frac{TE_n \cdot \exp\left(-TE_n/T_2^*\right)}{\sum_{i=1}^{N} TE_i \cdot \exp\left(-TE_i/T_2^*\right)} \tag{7}$$

T_2^*FIT-weighted combination

Finally, as proposed in the introduction, real-time T_2^*-mapping is made possible when using multi-echo fMRI. Here, the per-volume estimation of T_2^* at each voxel, termed $T_2^*FIT(t)$ (to our knowledge first defined by Power et al., 2018), can also be used as the weighting factor in a per-volume echo combination scheme:

$$w_n^{T_2^* FIT}(t) = \frac{TE_n \cdot \exp\left(-TE_n/T_2^* FIT(t)\right)}{\sum_{i=1}^{N} TE_i \cdot \exp\left(-TE_i/T_2^* FIT(t)\right)} \tag{8}$$

The per-volume nature of this echo combination scheme makes it ideal for use in both offline and real-time applications, when an a priori T_2^*-map (like the one used in Eq. (7)) is not available or not preferred. To the best of our knowledge, this T_2^*FIT-weighted combination approach has not been described previously in the literature

In the methods and results presented in this work, we compare metrics derived from standard single echo fMRI analysis to metrics derived from analysing T_2^*-weighted, tSNR-weighted, TE-weighted, T_2^*FIT-weighted, and the T_2^*FIT parameter time series, in both offline and per-volume scenarios.

3. Methods

In-depth descriptions of the participant details, ethics approval, experimental design, MRI protocol, preprocessing, and data quality can be accessed in the related data article (Heunis et al., 2020a). Summarising statements are provided below for the sake of completeness.

3.1. Participants

MRI and physiology data were collected from $N = 28$ participants (male=20; female=8; age = 24.9 ± 4.6 mean + standard deviation). The study was approved by the local ethics review board and all participants gave written consent for their data to be collected, processed and shared in accordance with a GDPR-compliant procedure.

3.2. Experimental design

A total of seven MRI acquisitions were collected during a single scanning session per participant. These acquisitions include, in order of acquisition:

1 A T1-weighted anatomical scan
2 *rest_run-1*: the first resting state run, eyes fixated on a white cross
3 *fingerTapping*: a right hand finger tapping functional task
4 *emotionProcessing:* a matching-shapes-and-faces functional task
5 *rest_run-2*: the second resting state run, eyes fixated on a white cross
6 *fingerTappingImagined:* an imagined finger tapping functional task
7 *emotionProcessingImagined:* a functional task to recall an emotional memory

All four task paradigms followed an ON/OFF boxcar design, starting with the OFF condition, with both conditions lasting 10 vol (= 20 s at TR = 2 s). The control (i.e. OFF) condition for the *fingerTapping* task was to focus on a small white cross on a black screen; for the *emotionProcessing* task the control condition was the shape-matching block; and for the *fingerTappingImagined* and *emotionProcessingImagined* tasks the control conditions were counting backwards, respectively, in multitudes of 7 and 9.

3.3. MRI protocol

MRI data were acquired on a 3 Tesla Philips Achieva scanner (software version 5.1.7) and using a Philips 32-channel head coil. A single T1-weighted anatomical image was acquired using a 3D gradient echo sequence (T1 TFE) with scanning parameters: TR = 8.2 ms; TE = 3.75 ms; flip angle = 8°; field of view = 240 × 240 × 180 mm; resolution = 1 × 1 × 1 mm; total scan time = 6:02 min.

All six functional MRI scans were acquired using a multi-echo, echo-planar imaging sequence with scanning parameters: TR = 2000 ms; TE = 14,28,42 ms (3 echoes); number of volumes = 210 (excluding 5 dummy volumes discarded by the scanner); total scan time = 7:00 min (excluding 5 dummy volumes); flip angle = 90°; field of view = 224 × 224 × 119 mm; resolution = 3.5 × 3.5 × 3.5 mm; in-plane matrix size = 64 × 64; number of slices = 34; slice thickness = 3.5 mm; interslice gap = 0 mm; slice orientation = oblique; slice order/direction = sequential/ascending; phase-encoding direction = A/P; SENSE acceleration factor = 2.5. Parts of the cerebellum and brainstem were excluded for some participants to ensure full coverage of the cortex and subcortical areas of interest. Echo times, spatial resolution, and the SENSE factor were tuned with the aim of improving spatial resolution and coverage while limiting the TR to maximum 2000 ms, including a maximum number of echoes, and keeping the SENSE factor low to prevent SENSE artefacts.

In addition, cardiac and respiratory fluctuations were recorded during the functional scans, respectively using a pulse oximeter fixed to the participant's left index finger, and a pressure-based breathing belt strapped around the participant's upper abdomen. These were sampled at 500 Hz.

3.4. Data analysis

Data analysis consists of anatomical and functional preprocessing, definition and calculation of echo combination weights, multi-echo combination, time-series processing and calculation of comparison metrics.

All analyses are done on an individual basis (i.e. participant-specific), unless otherwise stated, to describe the effects and facilitate the use of these methods in real-time fMRI use cases.

All processing steps below were done using the open source MATLAB-based and Octave-compatible *fMRwhy* toolbox (v0.0.1; https://github.com/jsheunis/fMRwhy), which has conditional dependencies:

- *SPM12* (r7771; https://github.com/spm/spm12/releases/tag/r7771; Friston et al., 2007)
- *bids-matlab (v.0.0.1,* https://github.com/jsheunis/bids-matlab/releases/tag/fv0.0.1*)*
- *Anatomy Toolbox* (v3.0; Eickhoff et al., 2005)
- *dicm2nii* (v0.2 from a forked repository; https://github.com/jsheunis/dicm2nii/releases/tag/v0.2)
- *TAPAS PhysIO* (v3.2.0; https://github.com/translationalneuromodeling/tapas/releases/tag/v3.2.0; Kasper et al., 2017)
- *Raincloud plots* (v1.1 https://github.com/RainCloudPlots/RainCloudPlots/releases/tag/v1.1; Allen et al., 2019).

All data analysis scripts can be accessed for reproducibility or reuse with attribution at https://github.com/jsheunis/rt-me-fMRI.

3.4.1. Preprocessing

The basic anatomical and functional preprocessing pipeline applied to all data is described in detail in the data article, and included:

1 Defining a functional template from Echo 2 of the first volume of the first resting state run. Echo 2 is selected in order to apply the same pipeline and allow a fair comparison of multi-echo to single-echo data, since for the latter only a single time series similar to Echo 2 would be available.
   a Mapping prior data to the subject functional space, including:
   b Coregistration of the anatomical image and atlas-based regions of interest (available in MNI152 space; Eickhoff et al., 2005) to the functional template space, and resampling these to the functional resolution.
2 Tissue-based segmentation of the coregistered anatomical image (after coregistration but before downsampling) and subsequent definition of binary maps for grey matter, white matter, cerebrospinal fluid (CSF) and the whole brain.
3 Basic functional preprocessing steps, including: estimating realignment parameters from the Echo 2 time series, running slice timing correction on all echo time series, applying realignment parameters to all echo time series, and applying spatial smoothing (7 mm isotropic, i.e. twice the voxel width) to all echo time series.
4 Generating data quality control metrics and visualisations to allow inspection of the quality of anatomical and functional data and their derivatives.

Two aspects of the preprocessing and analyses pipelines are worth highlighting in the context of this study. Firstly, while an important focus for this work is its application and utility in real-time scenarios, all processing was done offline, either on the full dataset or on a per-volume (i.e. simulated real-time) basis. This was viable since the study did not include any neurofeedback or real-time adaptive paradigms that would have required real-time computation and interaction. Secondly, in order to use a standardised pipeline (across multiple runs of multi-echo and single-echo data) that can compute derivative measures that are aligned across analyses and therefore comparable on a per-voxel basis, we followed the concept of "minimally processed" data as described by DuPre et al. (2020). This means that minimal steps including slice timing correction and 3D volume realignment are applied to multi-echo data before decay parameter estimation or multi-echo combination.

3.4.2. Data quality control

The *fMRwhy* toolbox has a BIDS-compatible data quality pipeline for functional and anatomical MRI, *fmrwhy_bids_workflowQC*, that can be run automatically for a full BIDS-compliant dataset. After running minimal preprocessing steps it generates a subject-specific HTML-report with quality control metrics and visualisations to allow inspection of the data and its derivatives. Individual reports can be accessed in the derivatives directory of the shared BIDS-compliant dataset of this study (see Heunis et al., 2020a for details). Additionally, a web-application named ***rt-me-fMRI*** is provided along with this work and accessible at: https://rt-me-fmri.herokuapp.com/. It can be used interactively to explore various summaries of data quality metrics, including distributions of framewise displacement (FD) and tSNR, and physiology recordings, as well as the results of this study.

None of the participant datasets were excluded after inspection of the included quality metrics, even in cases of more than average or severe motion (specifically sub-010, sub-020, and sub-021), since such data could still be useful for data quality related insights or for future denoising methods validation. In addition, for all participant data the alignments of the anatomical masque, the derived tissue segmentation masks, and the EPI data were visualised, inspected and the overlap was found acceptable.

3.4.3. Multi-echo combination

Existing weighting parameters or parameter maps are required to allow both offline and per-volume combination of multi-echo data. Of the previously reported options for weighting schemes given in Section 2.2, the simplest option used in this study is the echo time (Eq. (5)) derived from the functional MRI protocol, which yields a TE-weighted combination. Other prior weighting parameters are calculated using the first resting state functional scan. For each minimally preprocessed echo time series of the resting state run, the time series mean and standard deviation are calculated. The mean divided by the standard deviation yields the temporal signal-to-noise ratio (tSNR), per echo, that is used as another weighting parameter (Eq. (4)) described as the PAID method by Poser et al. (2006). Additionally, the mean images from the three echo time series are used to derive the per-voxel estimates of S_0 and T_2^* assuming a mono-exponential decay model and using a log-linear regression estimation (Eq. (2)). This baseline T_2^* map can be used for T_2^*-weighted combination (Eq. (7)), described as optimal combination by Kundu et al. (2012). Lastly, the same log-linear regression that is applied to the time series mean images can also be applied to a single volume of any multi-echo data. This implies that the three echo images of any volume can be used as data points to estimate per-volume and per-voxel parameter maps, S_0FIT(t) and $T_2^*FIT(t)$, which in turn can be used for per-volume multi-echo combination (Eq. (8)), hereinafter referred to as T_2^*FIT-combination.

Multi-echo combination schemes are applied to all functional data excluding the first resting state run, from which prior baseline weight maps are derived. In sum, six time series are computed per functional run (as described in Fig. 2): Echo 2, tSNR-combined, TE-combined, T_2^*-combined, T_2^*FIT-combined, and the T_2^*FIT time series.

3.4.4. Time series processing

After computing the six time series per functional run (excluding the first resting state run), each resulting time series is processed as summarised in the bottom row of Fig. 2.

First, the tSNR of each time series is calculated prior to any further processing. Then, each time series is spatially smoothed using a Gaussian kernel with FWHM at 7 mm (i.e. double the voxel size). This is followed by participant-level GLM-based analysis of the four task runs. Task regressors included the main "ON" blocks for the *fingerTapping*, *fingerTappingImagined* and *emotionProcessingImagined* tasks, and both the separate "SHAPES" and "FACES" trials for the *emotionProcessing* task. Regressors not-of-interest for all runs included six realignment parameter time series and their derivatives, the CSF compartment time series, and RETROICOR regressors (both cardiac and respiratory to the 2nd order, excluding interaction regressors).

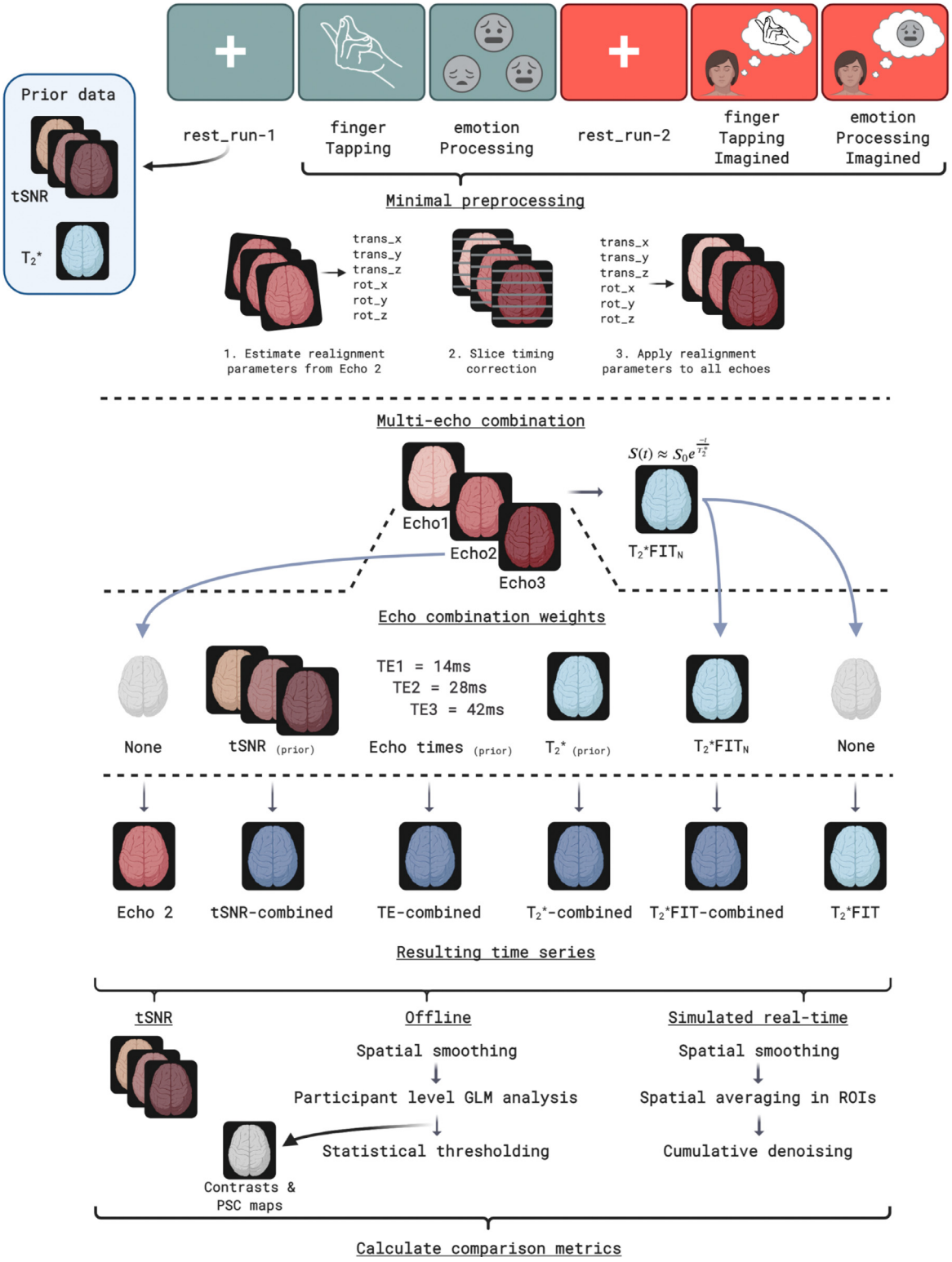

Fig. 2. The analysis pipeline applied to the rt-me-fMRI dataset. Prior tSNR and T_2^* maps are derived from the first resting state run. For all other functional runs (top row), six steps are executed per volume after minimal preprocessing in order to yield resulting multi-echo-derived time series for comparison: (1) the 2nd echo time series is extracted without processing, (2) the prior tSNR-weighted combination, (3) the TE-weighted combination, (4) the baseline T_2^*-weighted combination, (5) the T_2^*FIT-weighted combination, and (6) T_2^*FIT time series. Following this, each of the six time series then undergoes offline and simulated real-time processing pipelines. The offline pipeline includes (in order): tSNR calculation, spatial smoothing, participant-level task analysis, calculation of percentage signal change effect sizes, and statistical thresholding of the participant-level contrast maps. The simulated real-time pipeline is run per volume for each time series and includes (in order): spatial smoothing, spatial averaging of the appropriate region-of-interest signals, and cumulative denoising (including detrending using linear and quadratic regressors).

Additional steps executed by SPM12 before beta parameter estimation include high-pass filtering using a cosine basis set and AR(1) autoregressive filtering of the data and GLM design matrix. Contrasts are applied to the task-related beta maps for the *fingerTapping, fingerTappingImagined* and *emotionProcessingImagined* tasks, and to the FACES, SHAPES, and FACES>SHAPES beta maps for the *emotionProcessing* task. In order to yield a standard measure of effect size, the parameter estimates or contrast maps are then used to calculate percentage signal change (PSC) using the method described by Pernet (2014) and given by:

$$PCS = \frac{\hat{\beta}_{condition} * SF * 100}{\hat{\beta}_{constant}} \tag{9}$$

where $\beta_{condition}$ and $\beta_{constant}$ are parameter estimates corresponding to the relevant GLM regressors that are scaled with regards to the actual BOLD magnitude. To account for this, the scaling factor (*SF*) is determined as the maximum value of a reference trial taken at the resolution of the super-sampled design matrix X_{ss} (where supersampling is typically done before convolution with the hemodynamic response function):

$$SF = max\left(TrialX_{ss}\right) \tag{10}$$

Statistical thresholding was applied to identify task-related regions of activity by controlling the voxel-wise familywise error rate (FWE), with pFWE < 0.05, and a voxel extent threshold of 0.

3.4.5. Real-time analysis

Minimally processed time series are also analysed per-volume (using data acquired up to each volume in time) in order to explore multi-echo related BOLD sensitivity changes for real-time applications. Real-time analysis typically involves minimal processing (including 3D realignment), spatially averaging the signal within given ROIs, and additional per-volume denoising steps on the averaged signal. Here, we run a per-volume denoising process adapted from OpenNFT (Koush et al., 2017) on all task time series. This process is depicted in the bottom row of Fig. 2 and includes, in order: 1) Spatial smoothing using a Gaussian kernel with FWHM at 7 mm, 2) Spatial averaging of voxel signals with defined ROIs, and 3) Cumulative GLM-based detrending of the ROI signals, including linear and quadratic trend regressors. This then yields per-volume minimally denoised ROI-signals from which percentage signal change or another calculation can be used as the basis for the neurofeedback or real-time ROI signal.

3.4.6. Comparison metrics

To explore the differences between various multi-echo combinations and standard single echo data, and to investigate the usefulness of the former over the latter, we employ several comparison metrics:

- **Temporal signal-to-noise ratio (tSNR)** calculated as the voxel-wise time series mean divided by voxel-wise time series standard deviation. tSNR is an indicator of the amount of signal available from which to extract potentially useful BOLD fluctuations. Additionally, tSNR maps can be a robust visual indicator of increases or decreases in signal dropout.
- **Percentage signal change (PSC)** of task-based contrast maps resulting from participant-level GLM analysis. PSC represents a standardised measure of effect size (which beta or contrast values are not) and is an indicator of the BOLD sensitivity of the data based on GLM analysis.
- **T-statistic values** related to the task-based contrast maps resulting from participant-level GLM analysis.
- **Temporal percentage signal change (tPSC)** of the single echo, combined-echo and derived time series data of the task runs. This is calculated per voxel on minimally processed task data as the per-volume signal's percentage signal change from the time series mean (or, for real-time scenarios, from the mean of the preceding baseline "OFF" block or the cumulative mean). These are then spatially averaged within the regions listed below to yield ROI-based time series. These time courses are similar to what would be calculated in real-time as the ROI-based neurofeedback signal, and their amplitudes can be an indicator of BOLD sensitivity.
- **Functional contrast** of the ROI-based tPSC signals. To calculate the functional contrast in ROIs, the average tPSC in volumes classified as being part of "OFF" condition blocks are subtracted from the average signal in volumes classified as being part of each "ON" condition block. Visually, this corresponds to the average amplitude difference between conditions in the tPSC signal. The functional contrast is an indicator of the BOLD sensitivity of a signal based on both minimally processed and denoised data.
- **Temporal contrast-to-noise ratio (tCNR)** of the single echo, combined-echo and derived time series data of the task runs. To calculate the tCNR, the functional contrast in an ROI is divided by the time series standard deviation of the tPSC signal in the same ROI. This is related to both the tSNR and BOLD sensitivity. Where tPSC consists of time courses, tCNR provides a single summary value per voxel or region.

Extracting and spatially averaging voxel time series from specific regions is a common approach to exploring patterns of task-based activity in fMRI (Poldrack, 2007). This can be done both offline on a full dataset, and in real-time on the data as they are acquired. In this work, we explore and compare the above-mentioned metrics on both whole-brain and region-specific levels. Regions include:

- Grey matter (**GM**), white matter (**WM**) and cerebrospinal fluid (**CSF**) compartments. This allows quantifying, for example, whether combined multi-echo data changes a given metric similarly or differently across tissue types.
- A binary map of the voxels surviving voxel-wise pFWE <0.05 statistical thresholding (**FWE**). These maps vary spatially per time series of a given task run and they represent the functionally most responsive voxels based on the underlying data but assuming shared criteria (i.e. statistical threshold).
- A binary map resulting from a logical OR of the FWE-thresholded maps of all six time series of a given task run (**FWE-OR**). This allows the comparison of metrics in a region that includes the voxels that are judged to be significantly active in *any time series*, thus removing time series-specific spatial bias.
- Atlas-based anatomical regions of interest (**Atlas-based ROI**), derived from templates in MNI152 space (Eickhoff et al., 2005) that have been mapped to individual anatomical scans and coregistered and resampled to the individual functional space. This allows quantification of the above metrics within an a priori defined ROI, thus excluding spatial bias introduced by statistical thresholding. The Atlas-based ROIs include the **left motor cortex** (for right-hand finger tapping), and the **bilateral amygdala** (for emotion processing).

The focus of this work is on exploring, quantifying and describing differences and on generating data that allows deriving clear hypotheses for future confirmatory follow-up. While null hypothesis significance testing is used where necessary in task-based analysis, overall differences in the above-mentioned comparison metrics are not significance tested and are rather described in terms of means and percentage change from a reference.

4. Results

A web-application named ***rt-me-fMRI*** is provided alongside this work and accessible at: https://rt-me-fmri.herokuapp.com/. This browser-based application can be used interactively to explore the summary and participant-specific results presented below, and is intended to serve as supplementary material to this work.

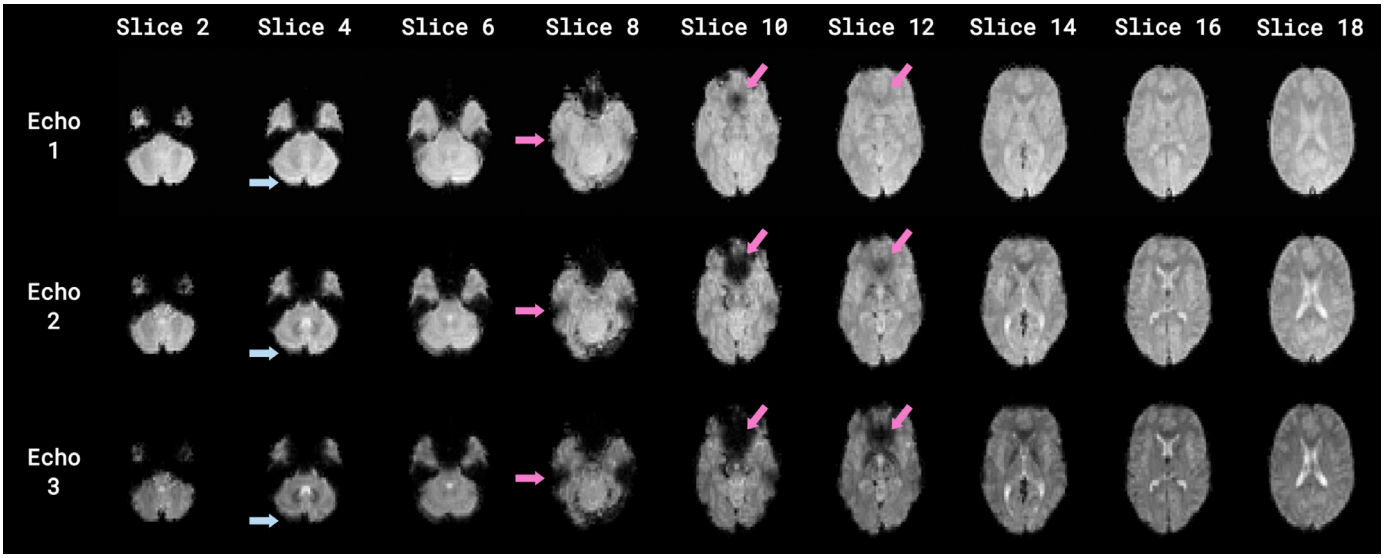

Fig. 3. Signal decay along the three echoes (top to bottom) of a single volume. Signal decay is displayed across a selection of slices (horizontal axis). Signal dropout is clearly evident in the orbitofrontal and ventromedial prefrontal cortices and inferior and anterior temporal lobes (magenta arrows; slices 8, 10, 12) and the cerebellum (light blue arrows; slices 2, 4, 6).

4.1. Multi-echo decay

To illustrate signal decay and dropout as a function of echo time, a simple plot of the inferior slices of a single subject is given in Fig. 3.

Signal decay can be seen clearly as the signal intensity diminishes from Echo 1 to Echo 3 (top to bottom) in all displayed slices. Signal dropout from Echo 1 through Echo 3 is particularly evident in the areas of the orbitofrontal and ventromedial prefrontal cortices, and the inferior and anterior temporal lobe (magenta arrows; slices 8, 10, 12) and the cerebellum (light blue arrows; slices 2, 4, 6).

4.2. Signal intensity, dropout, and temporal signal-to-noise ratio

We can visually inspect the effect on signal intensity and dropout when combining multi-echo data or deriving time series from it. Fig. 4A shows the mean of each of the six time series: Echo 2, T_2*-weighted combination, tSNR-weighted combination, TE-weighted combination, T_2*FIT-weighted combination, and T_2*FIT.

It is evident that most echo combination schemes, with the exception of TE-weighted combination, recover some signal lost due to dropout in the orbitofrontal and ventromedial prefrontal regions (magenta arrows; slices 8, 10) and inferior and anterior temporal regions (light blue arrows; slices 6, 8). This signal recovery is further demonstrated in the tSNR maps provided in Fig. 4B, particularly by the magenta arrows showing areas of signal dropout in Echo 2 and subsequent recovery in combined and derived time series tSNR maps. Even the T_2*FIT, for which the tSNR is evidently much lower than all other time series including Echo 2, recovers some of the signal that is lost due to low BOLD sensitivity in the affected areas, although signal loss is also more evident (slice 10). Additionally, tSNR in areas close to the bilateral temporal-occipital junction and towards the occipital lobe (Fig. 4B, green arrows) appears to increase substantially for all combined time series vs. Echo 2. This is more pronounced in the T_2*FIT-weighted compared to the T_2*-weighted and tSNR-weighted combinations, and less so in the TE-weighted combination.

To provide a more quantified view than these visualisations of signal intensity (Fig. 4A) and tSNR (Fig. 4B), distribution plots were created for grey matter tSNR values, both for the whole group and for subjects individually. These are accessible in the supplementary web-application, which shows (for example) for *sub-001_task-rest_run-2* a mean tSNR increase for all combined time series compared to Echo 2, with the T_2*FIT-weighted combination showing the largest increase (36.14%) and the T_2*FIT time series showing a substantial decrease (−55.89%). This generalises to the whole group (see Fig. 5A), i.e. a mean tSNR increase for all combined time series compared to Echo 2, with the T_2*FIT-weighted combination showing the largest increase (a comparable 36.95%). This increase in the tSNR of T_2*FIT-weighted combination replicates results that we previously reported on a different dataset (Heunis et al., 2019). This relationship also repeats for different regions, as can be seen for the left motor cortex (Fig. 5B) and the bilateral amygdala (Fig. 5C).

Note, however, that the mean tSNR values increase differentially based on the region. For the T_2*FIT-weighted combination, for example, whole brain data show a mean tSNR increase of 36.95%; the left motor cortex shows a mean tSNR increase of 31.63%; and the bilateral amygdala shows a mean tSNR increase of 53.35%. Other combined time series show percentage increases following the same pattern. This could be explained by the baseline T_2*-values in the motor cortex and the whole brain being closer to the time Echo 2 (28 ms) than the T_2*-values in the amygdala, i.e. that the T_2*-weighting of Echo 2 in those regions is already closer to optimal than the weighting of Echo 2 in the amygdala. This suggests that the amygdala and similarly affected areas with T_2*-values that are different from the average have more to gain from the multi-echo combination process.

Another noteworthy aspect is the low signal intensity and low tSNR of the T_2*FIT time series. The low signal intensity is explained by the fact that T_2*FIT values correspond to quantified units (ms) that are expected to be in a certain range (~ 0 to 120 ms for the human brain at 3T, Peters et al., 2007), while the intensity of the standard single and combined echo images are in analogue units determined by MRI hardware and software. The low tSNR of the T_2*FIT time series could be explained by an increase in time series standard deviation resulting from the log-linear fitting procedure on noisy data and only using the three echoes to fit the mono-exponential decay model per volume. This increase in time series noise becomes evident below when investigating T-statistic values related to task-analysis, and temporal percentage signal change.

Distributions of grey matter tSNR values are useful for inspecting differences in signal increases and dropout recovery between single-echo, multi-echo combined, and derived timeseries, and enable identifying new voxels or regions with adequate signal for task (or other) analysis. However, tSNR does not provide a direct measure of task sensitivity, i.e. it does not directly tell us whether newly recovered signal/regions

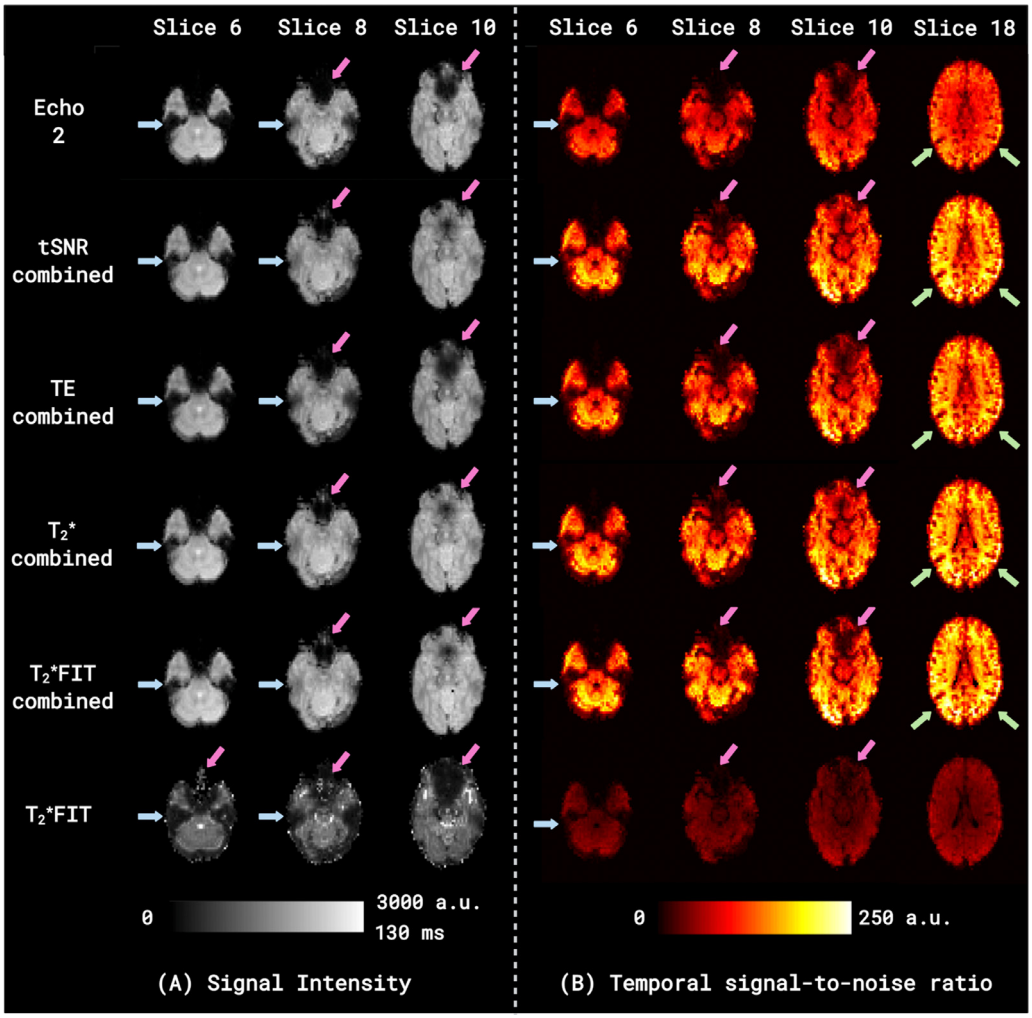

Fig. 4. Signal intensity (Fig. 4A) and Temporal signal-to-noise ratio (Fig. 4B) shown in mean images for the time series in rows from top to bottom: Echo 2, tSNR-weighted combination, TE-weighted combination, T2*-weighted combination, T2*FIT-weighted combination, and T2*FIT. Scaling for Fig. 4A is given both for the T2*FIT signal (0–130 ms) and for all the other signals (0–3000 a.u.). All echo combination schemes, with the exception of TE-weighted combination, recover some signal lost due to dropout in the orbitofrontal and ventromedial prefrontal regions (magenta arrows; slices 8, 10) and inferior and anterior temporal regions (light blue arrows; slices 6, 8). Slight signal recovery in T2*FIT is visible in the orbitofrontal and ventromedial prefrontal regions (slice 6) although signal loss is more evident in slice 10. In Fig. 4B, all time series apart from T2*FIT show increases in tSNR (from Echo 2) in areas close to the bilateral temporal-occipital junction and towards the occipital lobe (green arrows; slice 18), which is more pronounced in the T2*FIT-weighted compared to the T2*-weighted and tSNR-weighted combinations, and less so in the TE-weighted combination.

would be usefully related to the underlying task. For that reason, further measures derived from task analyses like the effect sizes, T-statistic values, and contrast to noise ratios are important to explore.4.4. Effect sizes and T-statistics

Fig. 6 shows distribution plots (over all subjects) of the mean PSC values within the respective **FWE-OR** regions for all task runs: *fingerTapping* (Fig. 6A), *fingerTappingImagined* (Fig. 6B), *emotionProcessing* (Fig. 6C), and *emotionProcessingImagined* (Fig. 6D). It is evident from Fig. 6A through 6D that the effect sizes show a substantial increase for the T_2*FIT time series (from Echo 2) in all tasks (respectively 87.91%, 67.86%, 13.51%, and 43.28%), while displaying a similar or decreased mean effect size for all combined times series. Data in the supplementary browser-based application also shows that this increase for T_2*FIT is more pronounced when looking at the effect sizes within their respective **FWE** regions (i.e. different activated voxels for each multi-echo derived time series, although mostly overlapping), which one should be wary of overinterpreting given the inherent circularity of re-analysing data in voxels that previously passed a significance threshold using the same data. On the other hand, this result is less pronounced for the time series effect sizes within their respective **atlas-based** regions of interest, mainly resulting in a longer tailed distribution of mean PSC values for the T_2*FIT time series. In some participants the mean PSC values of the T_2*FIT time series even show a slight decrease. These decreases in PSC disappear when looking at peak effect sizes, as opposed to mean effect sizes, in all regions of interest. Further differences can be inspected in depth using the supplementary browser-based application.

To accompany these effect size values, Fig. 7 shows distribution plots (over all subjects) of the mean T-statistic values in the respective **FWE-OR** regions for all task runs: *fingerTapping* (Fig. 7A), *fingerTappingImagined* (Fig. 7B), *emotionProcessing* (Fig. 7C), and *emotionProcessingImagined* (Fig. 7D). For all tasks, it is evident that resulting T-values for the combined echo time series are very similar in size and distribution to that of the Echo 2 time series, while T-values for the T_2*FIT time series are notably lower. The low mean T-values of T_2*FIT are due to the noise captured when estimating T_2* per-volume using only three data points, where noisy data would increase standard deviation and decrease the resulting T-values. This is substantiated by the large decrease in tSNR we saw for the T_2*FIT time series compared to that of the Echo 2 time

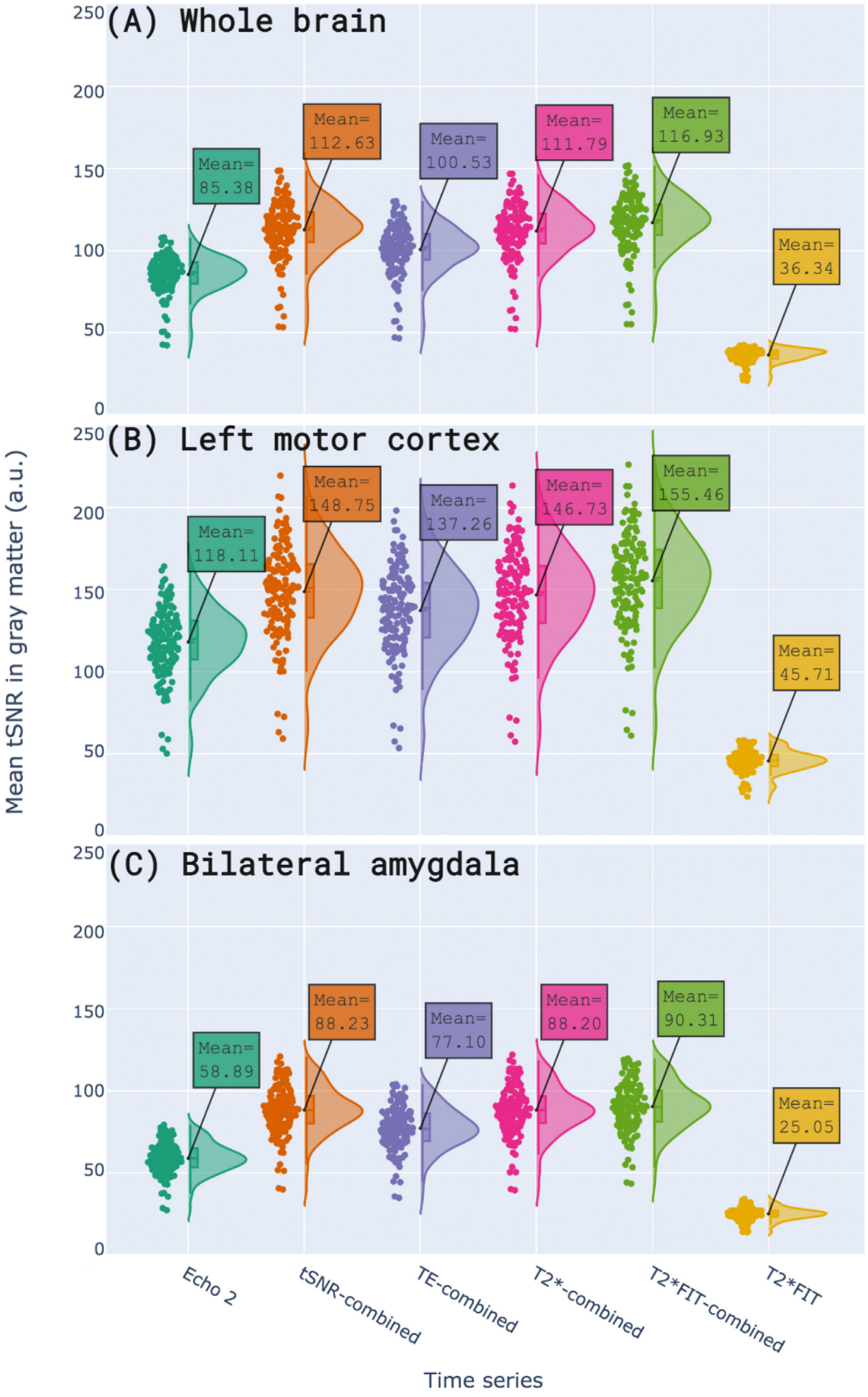

Fig. 5. Distribution / ridge plots of mean grey matter temporal signal-to-noise ratio (tSNR) over all participants and all runs. Plots are shown for (A) the whole brain, (B) the left motor cortex, and (C) the bilateral amygdala, each displaying a distribution for the six time series from left to right: Echo 2, tSNR-weighted combination, TE-weighted combination, T2*-weighted combination, T2*FIT-weighted combination, and T2*FIT. In all regions, the mean T2*FIT tSNR decreases from Echo 2 while the tSNR of all other time series increase, with the T2*FIT-weighted combination showing the largest increase in all regions. Notably, tSNR increases for all the combined echo time series are more substantial in the amygdala (C) than the other regions (A, B).

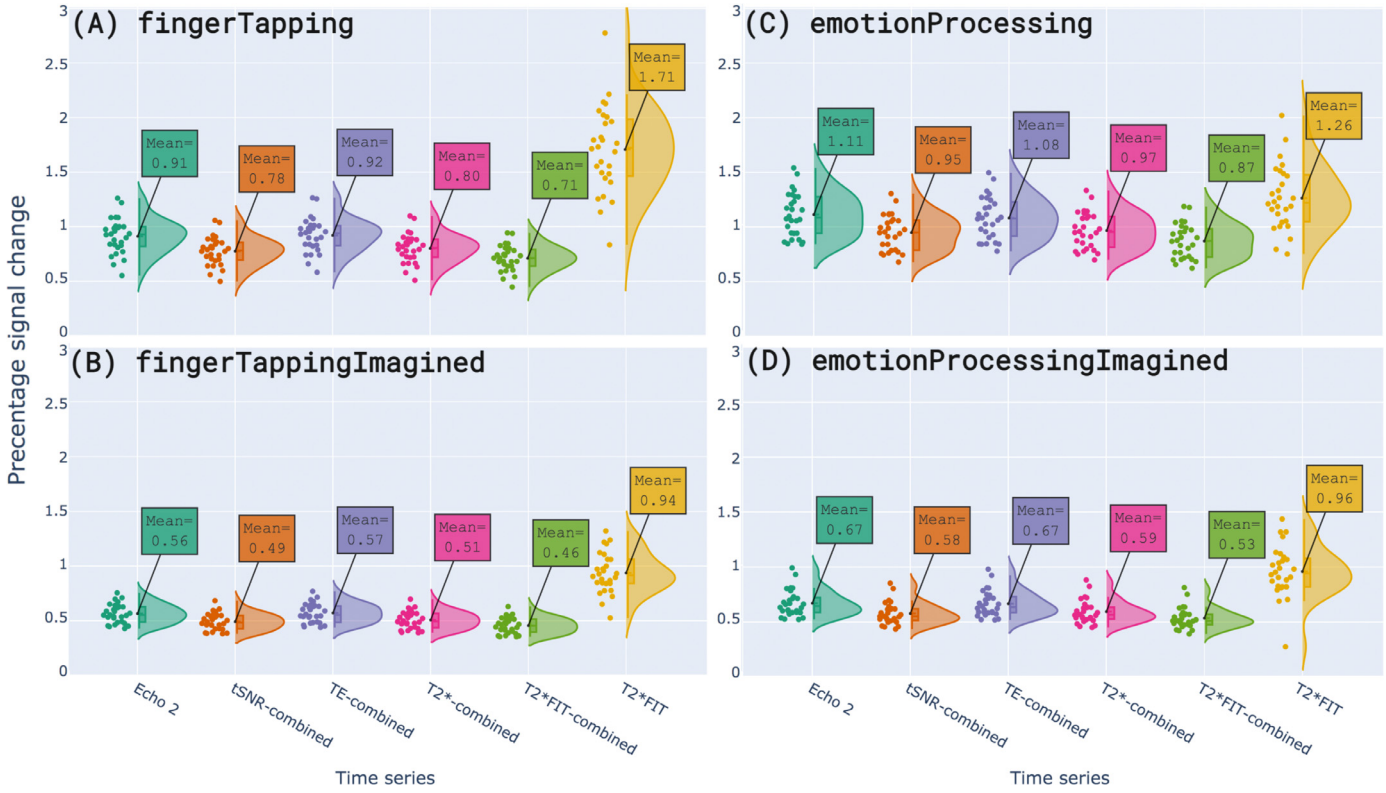

Fig. 6. Distribution plots of mean percentage signal change (PSC) values in the FWE-OR region for each of the four task runs. Plots from top to bottom are: (A) fingerTapping, (B) fingerTappingImagined, (C) emotionProcessing, and (D) emotionProcessingImagined. PSC values are shown for all six time series, from left to right: Echo 2, tSNR-weighted combination, TE-weighted combination, T2*-weighted combination, T2*FIT-weighted combination, and T2*FIT. For all tasks, the T2*FIT time series effect sizes show mean increases above the effect sizes of the Echo 2 time series, while all multi-echo combined time series effect sizes show similar or decreased means.

series in Figs. 4 and 5. Additionally, the TE-combined time series show slightly higher T-values for all tasks compared to other combined time series. However, this slight increase does not persist when analysing other regions (e.g. **FWE** or **atlas-based**) as can be viewed with the supplementary browser-based application.

4.5. Temporal percentage signal change and functional contrast

Temporal percentage signal change is useful to inspect the per-volume fluctuations of signal in task-related regions. This can be done for both offline and real-time scenarios but is particularly important for the latter in applications like region-based neurofeedback. tPSC in the offline scenario is calculated per volume from minimally processed data, yielding a per-voxel tPSC time series that can be depicted in a carpet plot for quality inspection or used for ROI analyses. tPSC for real-time scenarios is calculated from real-time minimally denoised *ROI-averaged signal* (with regards to the mean of the preceding baseline "OFF" block or with regards to the cumulative total or baseline mean) yielding the real-time ROI-signal typically used in region-based neurofeedback.

Here we focus on exploring tPSC and functional contrast for the real-time scenario. While offline tPSC is useful for post-hoc inspection of signal quality and task activity, it reflects similar data already presented above in the PSC and T-statistic distributions. Additionally, offline tPSC does not accurately reflect the effects seen for real-time scenarios where per-volume calculations can only use information available up to the most recently acquired volume. For that purpose, minimally processed data are cumulatively detrended and real-time tPSC is then calculated with regards to a cumulative baseline mean.

Fig. 8 shows functional contrast for all subjects calculated from real-time tPSC signals for the *fingerTapping* and *emotionProcessing* tasks, in the **FWE-OR** and **atlas-based** regions (the corresponding offline metrics can be inspected in detail in the supplementary web-application). The T_2*FIT signal clearly has a larger functional contrast (higher tPSC during task blocks and lower tPSC during resting blocks) than all other signals, for which the functional contrasts are very similar. For example, the minimum percentage increase of T_2*FIT functional contrast over Echo 2 functional contrast is 260.61% (from 0.33 to 1.19) in the **FWE-OR** region of the *emotionProcessing* task. Taking supplementary data into account, there is also an increased functional contrast for the real-time T_2*FIT time series compared to its offline counterpart.

A caveat here is that the T_2*FIT time series has the lowest tSNR of all time series, as noted in Fig. 5. In real-time scenarios, this could diminish the benefit of the high functional contrast in that the improved sensitivity to detect brain activity in an ROI would not necessarily be temporally stable. To take this into account, the functional contrasts are divided by the standard deviation of the tPSC time series to yield the temporal contrast-to-noise ratio (tCNR). This is shown for the **FWE-OR** regions in the *fingerTapping* and *emotionProcessing* tasks in Fig. 9 below, along with examples of single-participant real-time tPSC signals for the same tasks and regions. These plots highlight both functional contrast and volume-to-volume fluctuations.

Notably, the distributions in Fig. 9A and 9B show a substantial increase in tCNR for the T_2*FIT time series versus Echo 2 (97.78% for *fingerTapping* and 172.31% for *emotionProcessing*), while the distributions of all other multi-echo combined time series are very similar in shape and size to Echo 2. These promising results suggest that the decreased voxel-wise tSNR of the T_2*FIT time series is less detrimental on the level of the ROI-averaged signal. Offline tCNR calculations (accessible in the supplementary web-application) however show very similar tSNR distributions for all time series including T_2*FIT and Echo 2. On the level of individual ROI-averaged signals, Fig. 9C and 9D show tPSC signals in the FWE-OR regions, with higher amplitude differences for the T_2*FIT time

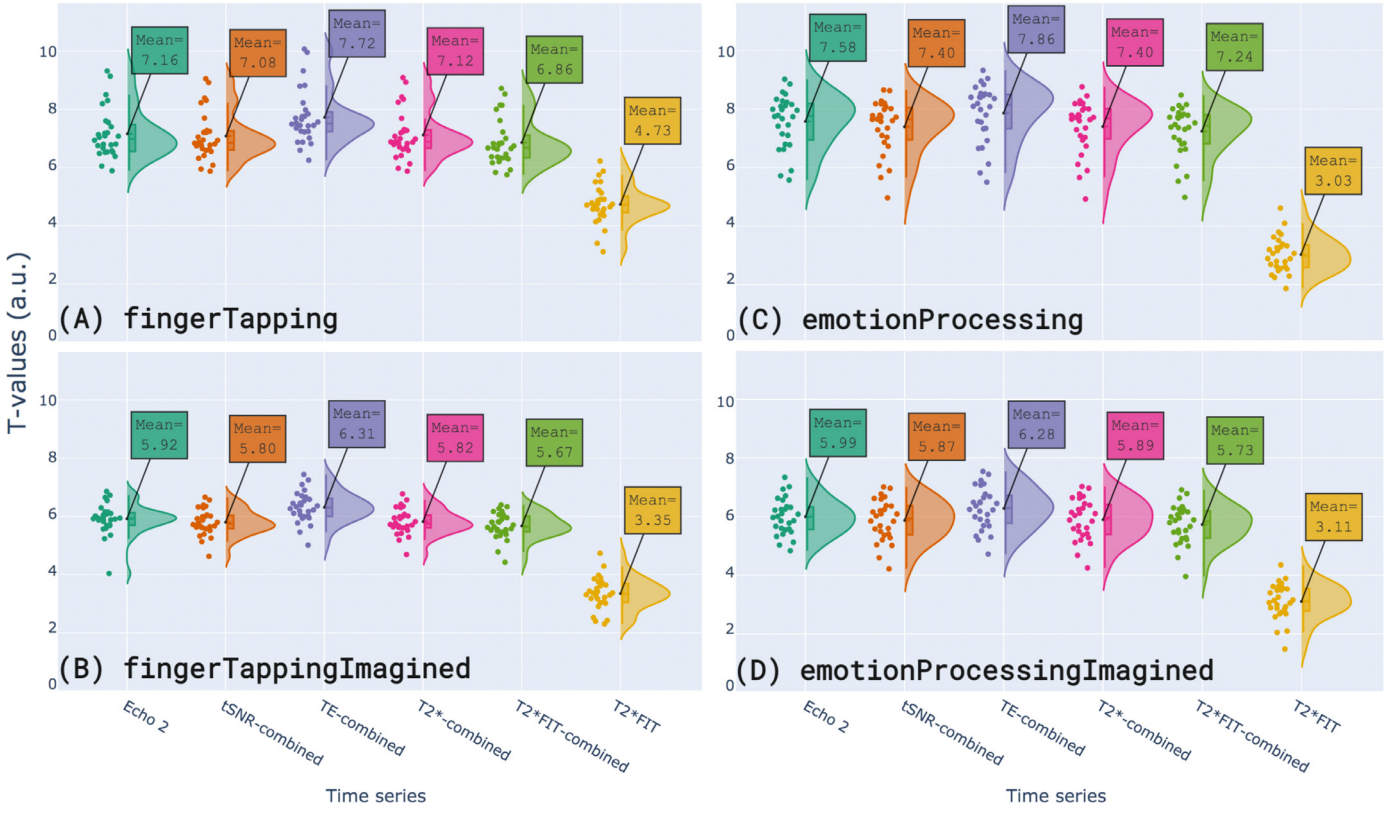

Fig. 7. Distribution plots of mean statistical T-values in the FWE-OR region for each of the four task runs. Plots from top to bottom are: (A) fingerTapping, (B) fingerTappingImagined, (C) emotionProcessing, and (D) emotionProcessingImagined. T-values are shown for all six time series, from left to right: Echo 2, tSNR-weighted combination, TE-weighted combination, T2*-weighted combination, T2*FIT-weighted combination, and T2*FIT. For all tasks, T-values of the combined echo time series are very similar in size and distribution shape to that of the Echo 2 time series, while T-values for the T2*FIT time series are notably lower.

series compared to all other time series, echoing the increased functional contrast seen for the group in Fig. 8. While a slight increase in volume-to-volume fluctuations relative to the signal amplitude is also visible, this does not substantially affect tCNR measures.

Another note regarding the tPSC signals shown in Figs. 9C and 9D is that these visualisations reflect temporally smoothed data, using a moving 3-point average. In real-time analysis it is common to apply a windowed averaging filter to the ROI time series in order to increase the tSNR, which improves the contrast and stability of the neurofeedback signal. This also improves our ability to classify individual volumes as a detected or undetected event of activity in cases where binary decision making is an important step for the specific real-time application. In the case of Fig. 9 it highlights the functional contrast improvement of the T_2*FIT time series. Note that the tCNR calculations that yielded the data of Fig. 8 were executed on temporally unsmoothed data. The supplementary web-application can be used to change views of the tPSC time series between temporally smoothed and unsmoothed visualisations.

5. Discussion

In this work we presented a comprehensive exploration and evaluation of existing and novel multi-echo combination and T_2*-mapping methods for both real-time and offline BOLD sensitivity improvements. A resting state and task-based healthy participant dataset was collected, curated and made available to the community for future investigations. In this dataset, we investigated five time series derived from multi-echo data and their differences from a single echo time series (Echo 2): tSNR-weighted combination, TE-weighted combination, T_2*-weighted combination, T_2*FIT-weighted combination, and the T_2*FIT time series. These differences were explored in terms of: temporal signal-to-noise ratio, percentage signal change as task-based effect size measure, offline and real-time temporal percentage signal change in regions of interest, functional contrast in ROIs, and temporal contrast-to-noise ratio in ROIs.

5.1. Results

Our results, across 28 participants, are summarised as follows. Dropout recovery is more pronounced (in orbitofrontal, ventromedial prefrontal regions as well as inferior and anterior temporal regions) for the T_2*-weighted, tSNR-weighted, and T_2*FIT-weighted combinations than for the TE-weighted combination. All multi-echo combined time series yield increases in tSNR compared to Echo 2, with the newly-proposed T_2*FIT-weighted combination resulting in the largest increase in mean tSNR. For the T_2*FIT-weighted combination, increases in mean tSNR are larger for the amygdala than for the left motor cortex or the whole brain. In contrast, the T_2*FIT time series results in a substantial mean decrease in tSNR from Echo 2. Alternatively, the T_2*FIT time series yields the largest effect size measures across all investigated functional tasks and regions, whereas the effect size measures derived from combined echo time series tend to decrease slightly from those of Echo 2, for all functional tasks. Based on temporal percentage signal change calculated offline from minimally processed data, the T_2*FIT time series yields the highest functional contrast for all tasks. Similarly, based on temporal percentage signal change calculated in simulated real-time from cumulatively denoised data, the T_2*FIT time series also yields the highest functional contrast for all tasks, although this increase is substantially more than the increase seen for its offline counterpart. For real-time scenarios, the temporal contrast-to-noise ratio of the T_2*FIT time series is notably higher than all other time series, which are very similar in size and distribution.

The fact that multi-echo combined time series yields increased tSNR compared to single echo data has been widely demonstrated in previ-

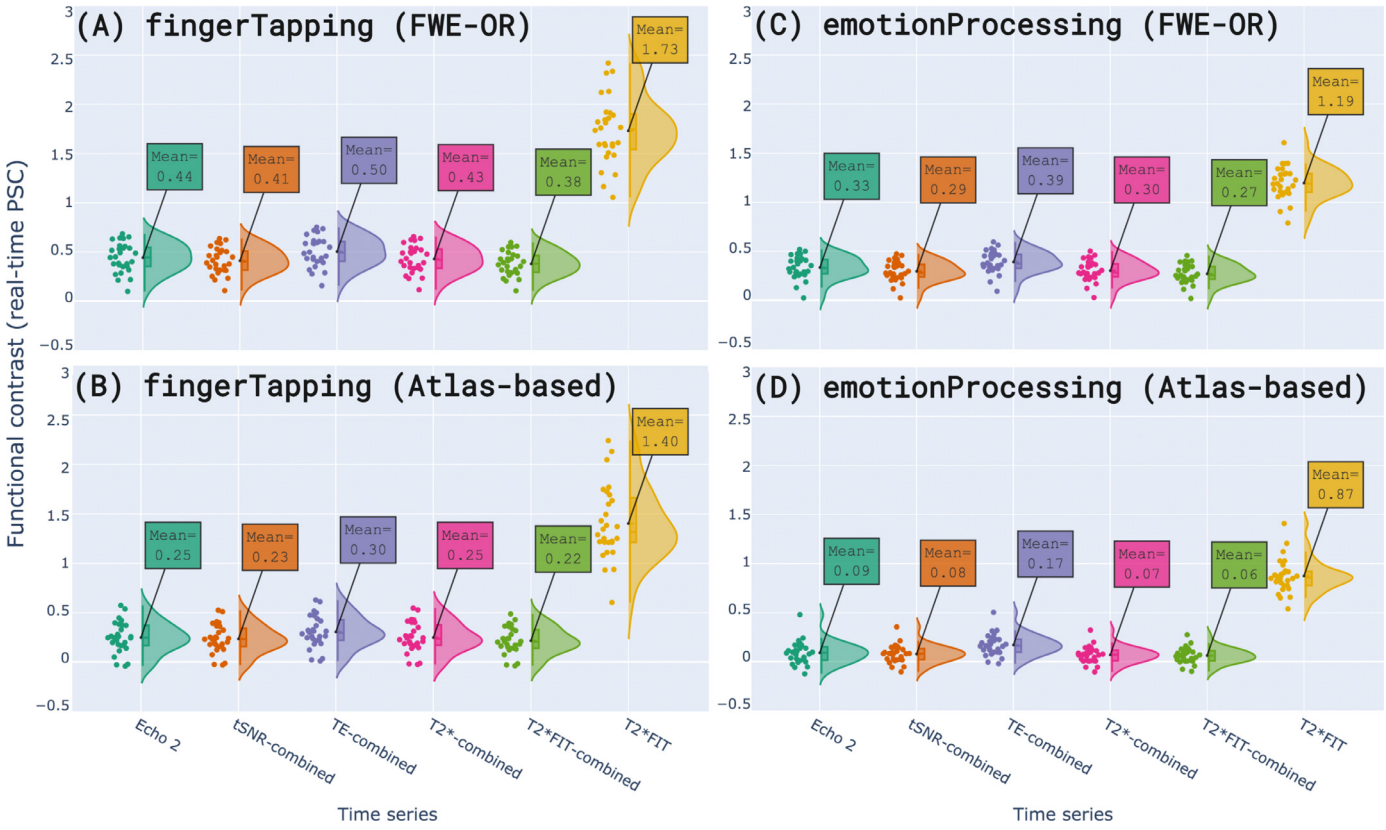

Fig. 8. Distributions of functional contrasts calculated from real-time temporal percentage signal change of the fingerTapping and emotionProcessing tasks. Contrast distributions are shown for both tasks within the FWE-OR region (A and C) and within the atlas-based region (B and D). Signals are colour coded for Echo 2, tSNR-weighted combination, TE-weighted combination, T2*-weighted combination, T2*FIT-weighted combination, and T2*FIT. Similar to the offline tPSC case, the functional contrast (in both tasks) for the T2*FIT time series is greater than the contrasts for all other time series, in both regions, although this is less pronounced for the emotionProcessing task than for the fingerTapping task. Notably, functional contrast for the real-time T2*FIT time series is substantially increased compared to its offline counterpart (see supplementary web-application). Functional contrast is presented as differences in percentage signal change (y-axes).

ous research, and has been repeated here for all combined time series with respect to Echo 2. Additionally, we show that the novel T_2*FIT-weighted combination yields the largest increase, replicating our previous results from a different dataset (Heunis et al., 2019). In the amygdala, a mean increase in tSNR of 53.35% was calculated across participants, while the mean increases for the left motor cortex and the whole brain were respectively 31.63% and 36.95%. These differences suggest that multi-echo combination, and in particular T_2*FIT-weighted combination, could prove more useful in terms of tSNR for areas traditionally suffering from suboptimal BOLD sensitivity due to their lower local baseline T_2*-values. On the other hand, improving tSNR in individual regions could also benefit whole-brain methods where spatially distributed ROIs or networks are used as the neurofeedback substrate (e.g. connectivity-based neurofeedback employed by Megumi et al., 2015, or default mode network-based neurofeedback employed by MacDonald, et al., 2017), since this would decrease spatial variability in BOLD effects and could lead to more accurate brain-wide estimates of interest. Note that we did not explore the approach of averaging the echoes (i.e. simple summation) as for instance originally proposed in Posse et al. (2001), but this approach has proven reduced BOLD sensitivity than the rest of combination approaches investigated here.

While not novel, an important aspect demonstrated here was the decrease in tSNR for the T_2*FIT time series, reported before by others including Kundu et al. (2017). Importantly, the fitting procedure used to estimate per-volume T_2*- and S_0-values (assuming a mono-exponential decay curve) yields noisy results that influence the amplitude of the signal fluctuations with respect to the mean, thus increasing the standard deviation and decreasing tSNR. The pitfalls of assuming mono-exponential (as opposed to multi-compartment) decay and using a fitting procedure with few data points (3 in this case) have been described before (Whittall et al., 1999) and remain applicable here. Future work should aim to exploit technical advances such as simultaneous multi-slice imaging to increase the number of echoes acquired per volume, while investigating more robust models of T_2*-decay.

While tSNR is a useful quantifier of relative spatial signal increases and dropout recovery, it does not directly measure or represent BOLD sensitivity. To investigate how multi-echo derived data could improve our ability to link BOLD changes to neuronal effects, we employed statistical task-analysis to yield effect size measures to show the benefits of rapid T_2*-mapping over single echo fMRI. For all tasks, the T_2*FIT time series consistently yielded the largest standardised effect size measures in terms of percentage signal change calculated offline from contrast maps after participant-level GLM analysis, while the effect sizes for multi-echo combined data decreased slightly. This phenomenon of decreased effect sizes has been reported before for both optimally combined as well as MEICA-denoised data by Gonzalez-Castillo et al. (2016). This was reported for 5 subjects performing an auditory task in a 20 s ON/OFF block paradigm similar to the one in this work. Gonzalez-Castillo et al. calculated per-volume T_2*-maps (i.e. T_2*FIT time series) using the same log-linear fitting approach but with only two echoes (TE = 31.7 ms and 49.5 ms), also in accordance with Beissner et al. (2010), and found that the activation extent, effect sizes and T-statistic values all decreased for the T_2* time series compared to the original single echo time series. In contrast, we observe that the effect sizes calculated from the T_2*FIT time series *increase*, while the related T-statistic values decrease (indirectly preempted by the decrease

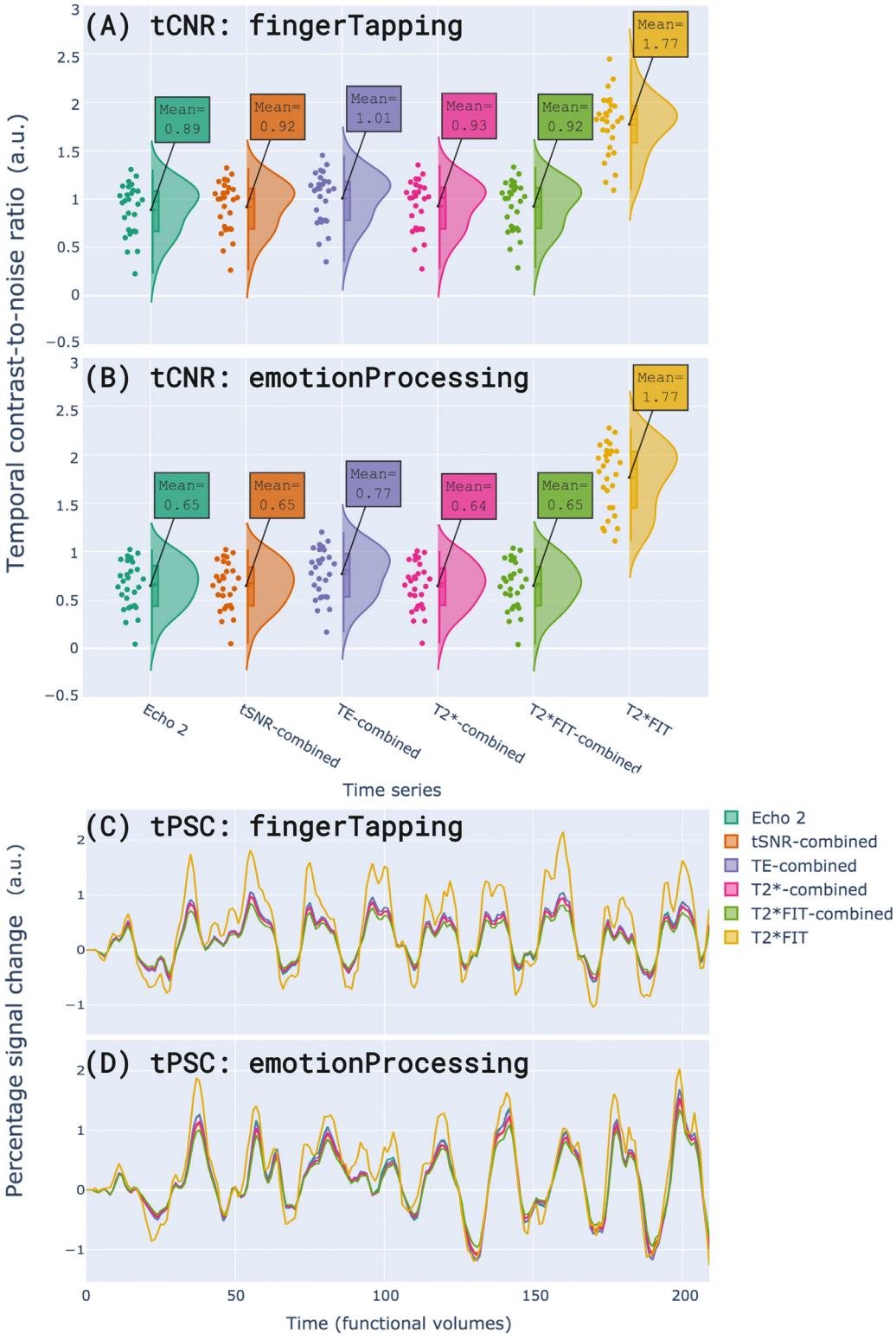

Fig. 9. Distributions of mean functional contrast-to-noise ratio (calculated from real-time temporal percentage signal change) of the (A) fingerTapping and (B) emotionProcessing tasks within the FWE-OR region. Subplots (C) and (D) show individual subject tPSC time series for the same tasks as mentioned, respectively, for (A) and (B). Signals are colour coded for Echo 2, tSNR-weighted combination, TE-weighted combination, T2*-weighted combination, T2*FIT-weighted combination, and T2*FIT. Since tCNR is computed from tPSC time series, the tCNR values computed from (C) and (D) represent a single data point per time series in subplots (A) and (B). The time series visualisations in (C) and (D) reflect temporally smoothed data, using a moving 3-point average. Transient fluctuations for the first two volumes in (C) and (D), ascribed to differences in calculating real-time tPSC (using the cumulative baseline mean) versus offline tPSC (using a full time series mean) were zeroed across all six time series in order to remove their biasing effects on tCNR calculations.

in tSNR). This difference in the change of the effect size with respect to Echo 2 might be explained by the use of three echoes in our calculation of the T_2*FIT time series, instead of two echoes, that could result in reduced accuracy of the T_2* estimates. This hypothesis can, in fact, be tested using the current *rt-me-fMRI* dataset, although that is considered beyond the scope of this work.

The T_2*FIT time series also consistently yielded the largest functional contrasts in terms of differences in task vs. baseline amplitudes in tPSC signals calculated from offline and real-time data. As an example, we observe an 87.91% increase in mean PSC (T_2*FIT compared to Echo 02) for the **FWE-OR** region of the *fingerTapping* task, and increases in functional contrast for the same task and region of 100% and 293%, respectively for offline and real-time scenarios. Interestingly, functional contrast for the real-time calculated tPSC signal showed an increase above the functional contrast calculated from offline data. The main mathematical difference in real-time vs offline approaches that this could be ascribed to is the cumulative calculation vs offline calculation, especially as regards the mean (cumulative baseline mean vs full time series mean). Beyond the functional contrast, the temporal contrast-to-noise ratio of the real-time tPSC signals were calculated to control for relative signal fluctuations, especially considering the low tSNR of T_2*FIT. Even so, the T_2*FIT time series consistently yielded the largest tCNR increase above Echo 2 for all tasks (e.g. 97.78% for the *fingerTapping* task), suggesting its benefits for improving BOLD sensitivity in real-time use cases.

This apparent contradiction of low tSNR versus high offline PSC and high real-time tCNR is worth exploring. Theoretically, we should expect an increase in BOLD sensitivity when analysing quantified T_2* fluctuations versus fluctuations in single echo image intensity, since the separation of T_2*- and S_0 should remove (to a considerable extent) system-level, inflow, and subject-motion effects from the T_2*-signal. What is left in the form of voxel-based T_2*FIT-values would then theoretically be more indicative of local neuronal activity than information derived from single echo data, assuming noise from the fitting procedure and other confounding factors do not attenuate this contrast substantially. Kundu et al. (2017) suggested that, even given a noisy fitting procedure, direct T_2* and S_0 fitting can be valid for separating low-frequency BOLD changes, while not ideal for higher frequency modulations that could alias with fitting error variations. In the task and ROI signal analyses presented here, as well as in the intended offline and real-time use cases of the presented methods, ON/OFF block paradigms generate slow BOLD changes where volume-to-volume fluctuations are averaged out to generate summary measures. This could explain, in part, the absence of detrimental effects resulting from the low tSNR. We also note that several levels of spatial smoothing applied to the real-time use case (whole volume spatial smoothing, followed by in-ROI voxel averaging) are bound to increase the tSNR of the ROI signal from which the tCNR is calculated. This likely counteracts the low tSNR of the T_2*FIT time series that conversely attenuates T-values in the offline use case. Additionally, acquisition parameters can have important influences on signal noise and parameter fitting error. Large voxel sizes (in this case 3.5 mm isotropic) are known to increase SNR and can be a contributing factor to the promising result reported in this work.

In terms of practical applicability to real-time fMRI research, we have shown the usefulness of multi-echo for real-time use cases in a 28-person dataset with several functional task designs. We demonstrate that real-time T_2*FIT-weighted combination yields brain wide mean tSNR increases and improves signal recovery in regions affected by dropout, compared to single echo and other combined multi-echo time series. We show additionally that the real-time T_2*FIT time series yields large functional contrast and tCNR increases compared to single echo or combined multi-echo time series. These improvements could benefit both real-time brain wide connectivity measures and real-time region-based signals, respectively, showing the possible utility for studies on adaptive paradigms and neurofeedback.

Lastly, we have shown that real-time multi-echo processing, specifically rapid T_2*-mapping and subsequent multi-echo combination is technically viable and practically supported. The software tools generated through this work (and shared with the community) support several per-volume or real-time multi-echo processing operations, including real-time 3D realignment of multi-echo data, real-time estimation of multi-echo decay parameters, real-time multi-echo combination using several weighting schemes, and multiple standard real-time preprocessing steps. It provides a practical toolkit for exploring real-time multi-echo fMRI data and for comparing the effects of acquisition and processing settings on BOLD sensitivity in individuals. Additionally, the interactive browser application allows easy access to the results (https://rt-me-fmri.herokuapp.com/), while the provision of supporting material and code (https://github.com/jsheunis/rt-me-fMRI) allows the presented results to be reproduced and allows replication attempts to be conducted on future datasets.

5.2. Limitations and future work

It remains important to consider caveats before further implementations and in order to direct future work. To start, we note that the *rt-me-fMRI* dataset does not include field maps and consequently no field map-based distortion correction steps were applied. To counter this absence, the alignments of the anatomical masque, as well as the derived tissue segmentation masks, and the EPI data were visualised, inspected and the overlap was found acceptable.

As regards the acquisition of a resting-state run from which to estimate T_2* before the start of a real-time session, future work could look into other acquisition types to improve the quality of prior T_2*-maps. For example, sequences like multi-echo GRE or ME-MP2RAGE (Metere et al., 2017; Sun et al., 2020), or multi-echo EPI sequences with a longer TR and more echoes, can all yield a more accurate T_2* estimation. Further changes to the acquisition strategy of the real-time runs may also benefit future applications. We mentioned voxel sizes above, but other aspects like increases in the number of receive coils, improvements in the implementation of acceleration techniques such as GRAPPA or SENSE, and field strength increases can all lead to lower levels of volume-to-volume noise and subsequent parameter estimations.

Regarding the exploration of tSNR improvements in multi-echo-derived data versus single-echo data, we note that these improvements can stem from different sources. For example, tSNR increases due to multi-echo weighting can originate from signal recovery (i.e. the mean signal owing to the first echo) or decrease of noise fluctuations due to the averaging. Additionally, tSNR changes could be different across brain regions and tissue types (for instance from grey versus white matter or CSF). Further work to delineate the exact origin of spatial variations of such tSNR improvements will allow future applications to gain use-case-specific benefits. Such investigations should also look closely at changes accompanying different acquisition strategies highlighted above.

In the described preprocessing pipeline, probabilistic cytoarchitectonic maps in MNI152 space (from Eickhoff et al., 2005) were co-registered to the subject functional space to create subject-specific regions of interest. It should be mentioned that these are less subject-specific than alternatives derived from individual anatomical features (such as those generated by the *freesurfer* software package), which points to an option for future improvement. Furthermore we note, as did Clare et al. (2001), that the selection of the region of interest within which to investigate activation effects, functional contrast, tSNR and more, can increase the variability of results and subsequent inferences. This issue was evaluated here considering three different ways of delineating the region of interest: **FWE, FWE-OR**, and **atlas-based**, and we observed attenuation of effect sizes, T-values and functional contrast as regions become less spatially matched to participants' functional activation localisation. This is particularly important for the real-time neurofeedback context, where a predefined subject-specific region of interest is often required to enable real-time region-based signal extraction. This concern about variability in the performance due to ROI definition extends to the implementation of real-time denoising steps as well, as

noted in our previous work on denoising steps in neurofeedback studies (Heunis et al., 2020b). In the current study, we intentionally implemented a minimal real-time processing pipeline to avoid confounding the results.

As summarised in the results discussion above, standardised effect sizes resulting from task analysis of all multi-echo combined time series were very similar in size and distribution, and on average much lower than that of the T_2^*FIT time series. This phenomenon could benefit from follow-up confirmatory analyses in a future study. Another claim that could be usefully extended into a follow-up investigation is the decision to include all participants in the study irrespective of the amount of motion in their data. As an example, some multi-echo combination schemes may be more or less robust to head motion, and the inclusion of all subjects would allow investigating such variations in higher versus lower motion subjects. Lastly, a key next step for extending the investigation of multi-echo use in offline task analysis is to examine activation clusters in more detail. This work looked at PSC and T-values in specific regions, but an important question to test would be whether multi-echo combined or derived times series yield activation clusters in new or unexpected brain regions, or how they affect existing activation clusters in terms of effect size and extent.

The supplementary web-application can also be seen as an evolving resource where other useful metrics, results and visualisations can be added in future. Examples of such additions include pairwise percentage differences in comparison metrics between the different multi-echo combined and derived time series and Echo 2; investigations into new or varying activation clusters resulting from multi-echo time series; or any other aspects covered here as future work.

While the presented benefits of multi-echo fMRI for real-time experiments are promising, further work is necessary to quantify the effects of a full multi-echo and real-time denoising pipeline on BOLD sensitivity and data quality. Taking into consideration the caveats discussed here, we advise researchers planning real-time fMRI studies to design and conduct effective pilot studies and to evaluate the effects robustly before deciding on the optimal multi-echo implementation settings

Credit-author-statement

Contributor Role	Role Definition	Contributor initials
Conceptualization	Ideas; formulation or evolution of overarching research goals and aims.	SH;
Data Curation	Management activities to annotate (produce metadata), scrub data and maintain research data (including software code, where it is necessary for interpreting the data itself) for initial use and later reuse.	SH;
Formal Analysis	Application of statistical, mathematical, computational, or other formal techniques to analyse or synthesize study data.	SH;
Funding Acquisition	Acquisition of the financial support for the project leading to this publication.	AA; RL;
Investigation	Conducting a research and investigation process, specifically performing the experiments, or data/evidence collection.	SH;
Methodology	Development or design of methodology; creation of models.	SH; WH; CC; LH; JJ;
Project Administration	Management and coordination responsibility for the research activity planning and execution.	SH; SZ;
Resources	Provision of study materials, reagents, materials, patients, laboratory samples, animals, instrumentation, computing resources, or other analysis tools.	SZ; AA; RL; MB;
Software	Programming, software development; designing computer programs; implementation of the computer code and supporting algorithms; testing of existing code components.	SH; RL;
Supervision	Oversight and leadership responsibility for the research activity planning and execution, including mentorship external to the core team.	AA; SZ;
Validation	Verification, whether as a part of the activity or separate, of the overall replication/reproducibility of results/experiments and other research outputs.	SH;
Visualization	Preparation, creation and/or presentation of the published work, specifically visualization/data presentation.	SH;
Writing – Original Draft Preparation	Creation and/or presentation of the published work, specifically writing the initial draft (including substantive translation).	SH;
Writing – Review & Editing	Preparation, creation and/or presentation of the published work by those from the original research group, specifically critical review, commentary or revision – including pre- or post-publication stages.	SH; SZ; AA; RL; MB; WH; CCG; LH; JJ

Declaration of Competing Interest

RL, WH, and MB are, respectively, employees of Philips Research and Philips Healthcare in The Netherlands. The other authors have declared that no further competing interests exist.

Acknowledgements

This work was funded by the foundation Health-Holland LSH-TKI (grant LSHM16053-SGF) and supported by Philips Research. LH was supported by the European Union's Horizon 2020 research and innovation program under the Grant Agreement no 794395. CCG was supported by the Spanish Ministry of Economy and Competitiveness (Ramon y Cajal Fellowship, RYC-2017- 21845), the Basque Government (PIBA_2019_104) and the Spanish Ministry of Science, Innovation and Universities (MICINN; PID2019-105520GB-100).

References

Allen, M., Poggiali, D., Whitaker, K., Marshall, T.R., Kievit, R.A., 2019. Raincloud plots: a multi-platform tool for robust data visualization. Wellcome Open Res. 4, 63. doi:10.12688/wellcomeopenres.15191.1.

Beissner, F., Baudrexel, S., Volz, S., Deichmann, R., 2010. Dual-echo EPI for non-equilibrium fMRI - implications of different echo combinations and masking procedures. Neuroimage 52, 524–531. doi:10.1016/j.neuroimage.2010.04.243.

Clare, S., Francis, S., Morris, P.G., Bowtell, R., 2001. Single-shot T measurement to establish optimum echo time for fMRI: studies of the visual, motor, and auditory cortices at 3.0 T. Magn. Reson. Med. 45, 930–933. doi:10.1002/mrm.1124.

Devlin, J.T., Russell, R.P., Davis, M.H., Price, C.J., Wilson, J., Moss, H.E., Matthews, P.M., Tyler, L.K., 2000. Susceptibility-Induced Loss of Signal: comparing PET and fMRI on a Semantic Task. Neuroimage 11, 589–600. doi:10.1006/nimg.2000.0595.

Dipasquale, O., Sethi, A., Laganà, M.M., Baglio, F., Baselli, G., Kundu, P., Harrison, N.A., Cercignani, M., 2017. Comparing resting state fMRI de-noising approaches using multi- and single-echo acquisitions. PLoS ONE 12, e0173289. doi:10.1371/journal.pone.0173289.

DuPre, E., Salo, T., Markello, R., Kundu, P., Whitaker, K., Handwerker, D., 2020. ME-ICA/tedana: 0.0.9a. Zenodo doi:10.5281/zenodo.3786890.

Eickhoff, S.B., Stephan, K.E., Mohlberg, H., Grefkes, C., Fink, G.R., Amunts, K., Zilles, K., 2005. A new SPM toolbox for combining probabilistic cytoarchitectonic maps and functional imaging data. Neuroimage 25, 1325–1335. doi:10.1016/j.neuroimage.2004.12.034.

Friston, K., Ashburner, J., Kiebel, S., Nichols, T., Penny, W., 2007. Statistical Parametric Mapping. Elsevier doi:10.1016/B978-0-12-372560-8.X5000-1.

Gonzalez-Castillo, J., Panwar, P., Buchanan, L.C., Caballero-Gaudes, C., Handwerker, D.A., Jangraw, D.C., Zachariou, V., Inati, S., Roopchansingh, V., Derbyshire, J.A., Bandettini, P.A., 2016. Evaluation of multi-echo ICA denoising for task based fMRI studies:

block designs, rapid event-related designs, and cardiac-gated fMRI. Neuroimage 141, 452–468. doi:10.1016/j.neuroimage.2016.07.049.

Gowland, P.A., Bowtell, R., 2007. Theoretical optimization of multi-echo fMRI data acquisition. Phys. Med. Biol. 52, 1801–1813. doi:10.1088/0031-9155/52/7/003.

Hagberg, G.E., Indovina, I., Sanes, J.N., Posse, S., 2002. Real-time quantification of T changes using multiecho planar imaging and numerical methods. Magn. Reson. Med. 48, 877–882. doi:10.1002/mrm.10283.

Heunis, J.S., Lamerichs, R., Song, G., Zinger, S., Aldenkamp, B., 2019. Improving BOLD sensitivity with real-time multi-echo echo-planar imaging - Towards a cleaner neurofeedback signal. In: Proceedings of the Benelux Chapter of the International Society for Magnetic Resonance in Medicine doi:10.5281/zenodo.2553256.

Heunis, S., Breeuwer, M., Gaudes, C.C., Hellrung, L., Huijbers, W., Jansen, J.F., Lamerichs, R., Zinger, S., Aldenkamp, A.P., 2020a. rt-me-fMRI: a task and resting state dataset for real-time, multi-echo fMRI methods development and validation. bioRxiv 2020.12.07.414490. https://doi.org/10.1101/2020.12.07.414490

Heunis, S., Lamerichs, R., Zinger, S., Caballero-Gaudes, C., Jansen, J.F.A., Aldenkamp, B., Breeuwer, M., 2020b. Quality and denoising in real-time functional magnetic resonance imaging neurofeedback: a methods review. Hum. Brain. Mapp. 41, 3439–3467. doi:10.1002/hbm.25010.

Kasper, L., Bollmann, S., Diaconescu, A.O., Hutton, C., Heinzle, J., Iglesias, S., Hauser, T.U., Sebold, M., Manjaly, Z.-.M., Pruessmann, K.P., Stephan, K.E., 2017. The PhysIO toolbox for modeling physiological noise in fMRI data. J. Neurosci. Methods 276, 56–72. doi:10.1016/j.jneumeth.2016.10.019.

Koush, Y., Ashburner, J., Prilepin, E., Sladky, R., Zeidman, P., Bibikov, S., Scharnowski, F., Nikonorov, A., De Ville, D.V., 2017. OpenNFT: an open-source Python/Matlab framework for real-time fMRI neurofeedback training based on activity, connectivity and multivariate pattern analysis. Neuroimage 156, 489–503. doi:10.1016/j.neuroimage.2017.06.039.

Kundu, P., Inati, S.J., Evans, J.W., Luh, W.-.M., Bandettini, P.A., 2012. Differentiating BOLD and non-BOLD signals in fMRI time series using multi-echo EPI. Neuroimage 60, 1759–1770. doi:10.1016/j.neuroimage.2011.12.028.

Kundu, P., Voon, V., Balchandani, P., Lombardo, M.V., Poser, B.A., Bandettini, P.A., 2017. Multi-echo fMRI: a review of applications in fMRI denoising and analysis of BOLD signals. Neuroimage 154, 59–80. doi:10.1016/j.neuroimage.2017.03.033.

Lombardo, M.V., Auyeung, B., Holt, R.J., Waldman, J., Ruigrok, A.N.V., Mooney, N., Bullmore, E.T., Baron-Cohen, S., Kundu, P., 2016. Improving effect size estimation and statistical power with multi-echo fMRI and its impact on understanding the neural systems supporting mentalizing. Neuroimage 142, 55–66. doi:10.1016/j.neuroimage.2016.07.022.

Marxen, M., Jacob, M.J., Müller, D.K., Posse, S., Ackley, E., Hellrung, L., Riedel, P., Bender, S., Epple, R., Smolka, M.N., 2016. Amygdala regulation following fMRI-neurofeedback without instructed strategies. Front. Hum. Neurosci. 10. doi:10.3389/fnhum.2016.00183.

McDonald, A.R., Muraskin, J., Dam, N.T.V., Froehlich, C., Puccio, B., Pellman, J., Bauer, C.C.C., Akeyson, A., Breland, M.M., Calhoun, V.D., Carter, S., Chang, T.P., Gessner, C., Gianonne, A., Giavasis, S., Glass, J., Homann, S., King, M., Kramer, M., Landis, D., Lieval, A., Lisinski, J., Mackay-Brandt, A., Miller, B., Panek, L., Reed, H., Santiago, C., Schoell, E., Sinnig, R., Sital, M., Taverna, E., Tobe, R., Trautman, K., Varghese, B., Walden, L., Wang, R., Waters, A.B., Wood, D.C., Castellanos, F.X., Leventhal, B., Colcombe, S.J., LaConte, S., Milham, M.P., Craddock, R.C., 2017. The real-time fMRI neurofeedback based stratification of Default Network Regulation Neuroimaging data repository. Neuroimage 146, 157–170. doi:10.1016/j.neuroimage.2016.10.048.

Megumi, F., Yamashita, A., Kawato, M., Imamizu, H., 2015. Functional MRI neurofeedback training on connectivity between two regions induces long-lasting changes in intrinsic functional network. Front. Hum. Neurosci. 9. doi:10.3389/fnhum.2015.00160.

Menon, R.S., Ogawa, S., Tank, D.W., Uğurbil, K., 1993. 4 Tesla gradient recalled echo characteristics of photic stimulation-induced signal changes in the human primary visual cortex. Magn. Reson. Med. 30, 380–386. doi:10.1002/mrm.1910300317.

Metere, R., Kober, T., Möller, H.E., Schäfer, A., 2017. Simultaneous quantitative MRI mapping of T1, T2* and magnetic susceptibility with multi-echo MP2RAGE. PLoS ONE 12, e0169265. doi:10.1371/journal.pone.0169265.

Moia, S., Termenon, M., Uruñuela, E., Stickland, R.C., Bright, M.G., Caballero-Gaudes, C., 2020. ICA-based denoising strategies in breath-hold induced cerebrovascular reactivity mapping with multi echo BOLD fMRI. bioRxiv doi:10.1101/2020.08.18.256479, 2020.08.18.256479.

Olafsson, V., Kundu, P., Wong, E.C., Bandettini, P.A., Liu, T.T., 2015. Enhanced identification of BOLD-like components with multi-echo simultaneous multi-slice (MESMS) fMRI and multi-echo ICA. Neuroimage 112, 43–51. doi:10.1016/j.neuroimage.2015.02.052.

Pears, J.A., Francis, S.T., Butterworth, S.E., Bowtell, R.W., Gowland, P.A., 2003. Investigating the BOLD effect during infusion of Gd-DTPA using rapid T mapping. Magn. Reson. Med. 49, 61–70. doi:10.1002/mrm.10340.

Pernet, C.R., 2014. Misconceptions in the use of the General Linear Model applied to functional MRI: a tutorial for junior neuro-imagers. Front. Neurosci. 8. doi:10.3389/fnins.2014.00001.

Peters, A.M., Brookes, M.J., Hoogenraad, F.G., Gowland, P.A., Francis, S.T., Morris, P.G., Bowtell, R., 2007. T2* measurements in human brain at 1.5, 3 and 7 T. Magnetic Resonance Imaging. Proceed. Int. Sch. Magn. Reson. Brain Funct. 25, 748–753. doi:10.1016/j.mri.2007.02.014.

Poldrack, R.A., 2007. Region of interest analysis for fMRI. Soc. Cogn. Affect. Neurosci. 2, 67–70. doi:10.1093/scan/nsm006.

Poser, B.A., Versluis, M.J., Hoogduin, J.M., Norris, D.G., 2006. BOLD contrast sensitivity enhancement and artifact reduction with multiecho EPI: parallel-acquired inhomogeneity-desensitized fMRI. Magn. Reson. Med. 55, 1227–1235. doi:10.1002/mrm.20900.

Posse, S., Binkofski, F., Schneider, F., Gembris, D., Frings, W., Habel, U., Salloum, J.B., Mathiak, K., Wiese, S., Kiselev, V., Graf, T., Elghahwagi, B., Grosse-Ruyken, M.-.L., Eickermann, T., 2001. A new approach to measure single-event related brain activity using real-time fMRI: feasibility of sensory, motor, and higher cognitive tasks. Hum. Brain. Mapp. 12, 25–41. doi:10.1002/1097-0193(200101)12:1<25::AID-HBM30>3.0.CO;2-H.

Posse, S., Fitzgerald, D., Gao, K., Habel, U., Rosenberg, D., Moore, G.J., Schneider, F., 2003. Real-time fMRI of temporolimbic regions detects amygdala activation during single-trial self-induced sadness. Neuroimage 18, 760–768. doi:10.1016/S1053-8119(03)00004-1.

Posse S, Wiese S, Kessler C, Gembris D, Weiss U, Peyerl M, Grosse-Ruyken ML, Elghawaghi B, Richards T, Dager S., 1998. Single Shot T2*-Sensitive Spectroscopic Imaging Increases fMRI Sensitivity: Preliminary Evidence from Visual and Olfactory Activation. Abstract book: International Society for Magnetic Resonance in Medicine.

Posse, S., Wiese, S., Gembris, D., Mathiak, K., Kessler, C., Grosse-Ruyken, M.-.L., Elghahwagi, B., Richards, T., Dager, S.R., Kiselev, V.G., 1999. Enhancement of BOLD-contrast sensitivity by single-shot multi-echo functional MR imaging. Magn. Reson. Med. 42, 87–97. doi:10.1002/(SICI)1522-2594(199907)42:1<87::AID-MRM13>3.0.CO;2-O.

Power, J.D., Plitt, M., Gotts, S.J., Kundu, P., Voon, V., Bandettini, P.A., Martin, A., 2018. Ridding fMRI Data of Motion-Related influences: Removal of Signals With Distinct Spatial and Physical Bases in Multiecho Data PNAS 201720985 doi:10.1073/pnas.1720985115.

Scheffler, K., Seifritz, E., Haselhorst, R., Bilecen, D., 1999. Titration of the BOLD effect: separation and quantitation of blood volume and oxygenation changes in the human cerebral cortex during neuronal activation and ferumoxide infusion. Magn. Reson. Med. 42, 829–836. doi:10.1002/(SICI)1522-2594(199911)42:5<829::AID-MRM2>3.0.CO;2-6.

Schulte, A.-.C., Speck, O., Oesterle, C., Hennig, J., 2001. Separation and quantification of perfusion and BOLD effects by simultaneous acquisition of functional I0- and T-parameter maps. Magn. Reson. Med. 45, 811–816. doi:10.1002/mrm.1109.

Sun, H., Cleary, J.O., Glarin, R., Kolbe, S.C., Ordidge, R.J., Moffat, B.A., Pike, G.B., 2020. Extracting more for less: multi-echo MP2RAGE for simultaneous T1-weighted imaging, T1 mapping, mapping, SWI, and QSM from a single acquisition. Magn. Reson. Med. 83, 1178–1191. doi:10.1002/mrm.27975.

Weiskopf, N., Klose, U., Birbaumer, N., Mathiak, K., 2005. Single-shot compensation of image distortions and BOLD contrast optimization using multi-echo EPI for real-time fMRI. Neuroimage 24, 1068–1079. doi:10.1016/j.neuroimage.2004.10.012.

Weiskopf, N., Suckling, J., Williams, G., Correia, M.M., Inkster, B., Tait, R., Ooi, C., Bullmore, E.T., Lutti, A., 2013. Quantitative multi-parameter mapping of R1, PD*, MT, and R2* at 3T: a multi-center validation. Front. Neurosci. 7. doi:10.3389/fnins.2013.00095.

Whittall, K.P., MacKay, A.L., Li, D.K.B., 1999. Are mono-exponential fits to a few echoes sufficient to determine T2 relaxation for in vivo human brain? Magn. Reson. Med. 41, 1255–1257. doi:10.1002/(SICI)1522-2594(199906)41:6<1255::AID-MRM23>3.0.CO;2-I.